Biosensors and Bioelectronics 132 (2019) 248–264

Contents lists available at ScienceDirect

Biosensors and Bioelectronics

journal homepage: www.elsevier.com/locate/bios

Current and future envision on developing biosensors aided by 2D molybdenum disulfide (MoS_2) productions

N. Dalila R[a], M.K. Md Arshad[a,b], Subash C.B. Gopinath[a,c], W.M.W. Norhaimi[b], M.F.M. Fathil[a]

[a] Institute of Nano Electronic Engineering, Universiti Malaysia Perlis, 01000 Kangar, Perlis, Malaysia
[b] School of Microelectronic Engineering, Universiti Malaysia Perlis, Pauh Putra, 02600 Arau, Perlis, Malaysia
[c] School of Bioprocess Engineering, Universiti Malaysia Perlis, 02600 Arau, Perlis, Malaysia

ARTICLE INFO

Keywords:
Molybdenum disulfide
Biosensors
2D Materials
Label-based
Label-free

ABSTRACT

Two-dimensional (2D) layered nanomaterials have triggered an intensive interest due to the fascinating physiochemical properties with the exceptional physical, optical and electrical characteristics that transpired from the quantum size effect of their ultra-thin structure. Among the family of 2D nanomaterials, molybdenum disulfide (MoS_2) features distinct characteristics related to the existence of direct energy bandgap, which significantly lowers the leakage current and surpasses other 2D materials. In this overview, we expatiate the novel strategies to synthesize MoS_2 that cover techniques such as liquid exfoliation, chemical vapour deposition, mechanical exfoliation, hydrothermal reaction, and Van Der Waal epitaxial growth on the substrate. We extend the discussion on the recent progress in biosensing applications of the produced MoS_2, highlighting the important surface-to-volume of ultrathin MoS_2 structure, which enhances the overall performance of the devices. Further, envisioned the missing piece with the current MoS_2-based biosensors towards developing the future strategies.

1. Introduction

The pioneering study of molybdenum disulfide (MoS_2) crystal structure was dated back in 1923 by Dickinson and Pauling (1923). Several layers, and the possible observation of monolayer was reported by Frindt and Yoffe (1963) in 1963 and the continuation of work from the same group has successfully demonstrated the identification of monolayer in 1986 (Joensen et al., 1986). However, the growth of interest in research only started after the discovery of graphene by Novoselov in 2004 (Novoselov et al., 2004). Since then, MoS_2 has attracted with a tremendous interest among researchers due to its fascinating characteristics that hold vast potentials in the fields of electronic, optical, mechanical and electrochemical (Choi et al., 2017; Li and Wong, 2017; Majd et al., 2018). These unique characteristics originate from the quantum size effect that results of their ultra-thin structure (Kalantar-Zadeh and Ou, 2016; D.-W. Lee et al., 2015). These material properties inherently exist as a two-dimensional transition metal, a typical example from the layered transition-metal dichalcogenide (TMDs) family (Radisavljevic et al., 2011). MoS_2 consists of S-Mo-S trilayered structure, which is separated via Van der Waals (Krishnamoorthy et al., 2016; Li and Zhu, 2015) and intrinsic electrical conductivity (Krishnamoorthy et al., 2016). In particular, $MoS_2$is one of the most stable transition metal dichalcogenides (TMDCs) (Majd et al., 2018) due to its versatile features (Marx et al., 2017). MoS_2 is configured in a honeycomb sheet with the transition metal atom Mo covalently sandwiched between two S atoms at two different possible edge terminations (Mahyavanshi et al., 2017). Most importantly, its ultrathin plane structure where the electrons/holes are confined to a plane of atomic thickness makes 2D MoS_2 sensitive to the surrounding environment (Chen et al., 2018). Therefore, to a large extent, 2D MoS_2 would be a promising building block for biosensors. The biosensor can be defined as devices to evaluate the specific biochemical reaction via bio-receptors for chemical compounds detection commonly by electrical, thermal or optical signals (IUPAC, 2014). Similar to the other 2D materials, MoS_2 promotes large surface areas and appreciable band gap (Majd et al., 2018), thus it is expected to surpass the graphene (zero band-gap) (Maidin et al., 2018) and graphene oxide in both electronics and optoelectronic-based applications (Kalantar-Zadeh and Ou, 2016; Wang et al., 2013). To emphasis on the bandgap, similar to other TMDs material, the MoS_2 have an electronic band structure which strongly depends on the number of layers. The bulk MoS_2 (2H-MoS_2) is a semiconducting material with an indirect bandgap of 1.2 eV (Ghasemi and Mohajerzadeh, 2016; Kalantar-Zadeh and Ou, 2016) whereas single-layer MoS_2 (1L-MoS_2) is a direct gap semiconductor with a bandgap of 1.8 eV (Ferrari et al., 2014; Lee et al., 2015; Radisavljevic et al., 2011; Roldan et al., 2017), thus very interesting for transistor

E-mail address: mohd.khairuddin@unimap.edu.my (M.K. Md Arshad).

https://doi.org/10.1016/j.bios.2019.03.005
Received 3 January 2019; Received in revised form 3 March 2019; Accepted 5 March 2019
Available online 06 March 2019
0956-5663/

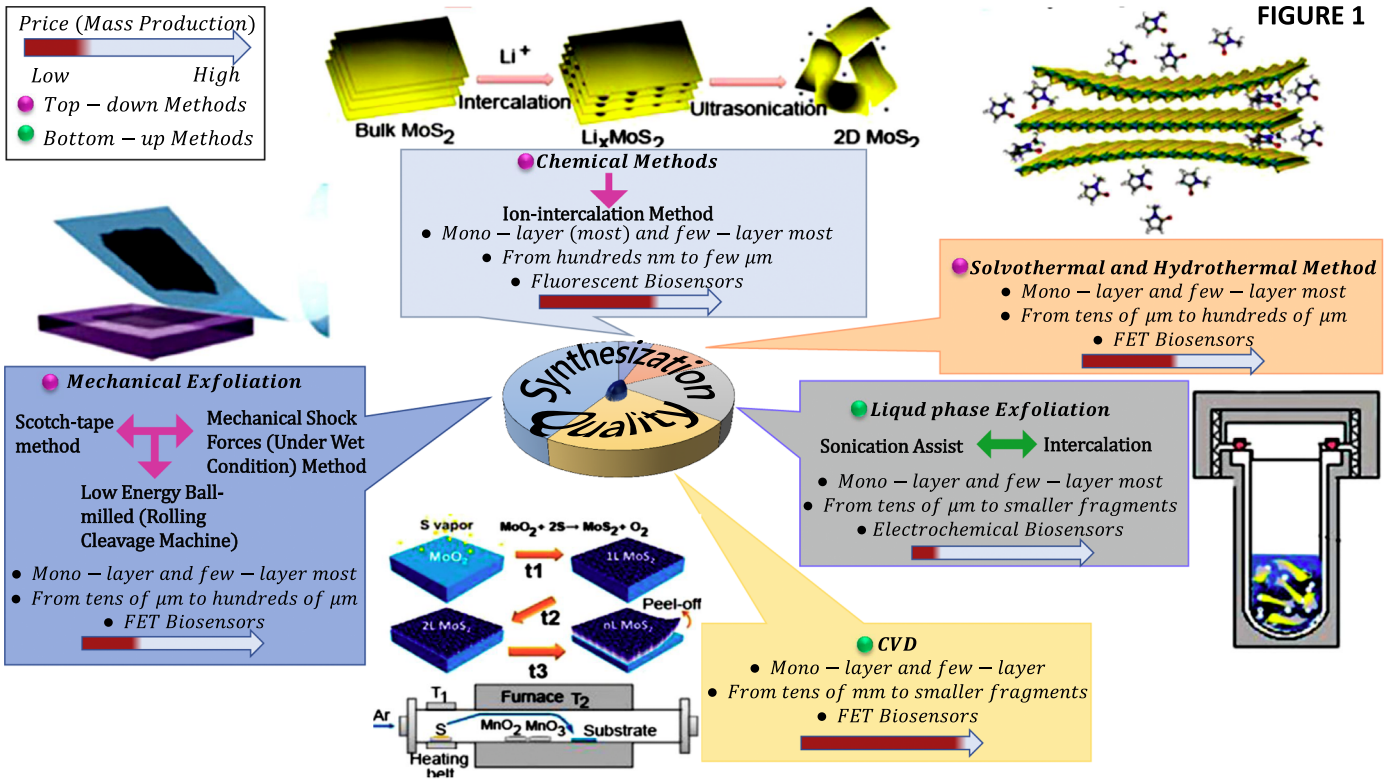

Fig. 1. An illustration to represent the comparison in term of quality and price (mass production) of five basic types of 2D material synthesization from a higher quality to the lower quality, which are mechanical exfoliation, chemical vapour deposition (CVD), liquid phase exfoliation, solvothermal/hydrothermal method, and chemical methods (Gan et al., 2017). Copyright 2016 Elsevier B. V.

applications (Radisavljevic et al., 2011) and demonstrated for microprocessor (Wachter et al., 2017).

As shown in Fig. 1, various methods to synthesis the two-dimensional (2D) MoS_2 have been reported (Gan et al., 2017). Different synthetisation methods, might exhibit different structural characteristics, which translates into different physical, electronic, chemical and surface properties. Thus, a comprehensive and appropriate characterization is very important and crucial.

2D MoS_2 becomes recent exuberant attention on developing the biosensors, thanks to its atomically thin-layer characteristics, which expected to provide a higher surface-to-volume ratio. Interaction of biomolecules on the surface plays a vital role in the development of a highly sensitive sensing platform (Ibau et al., 2017). As 2D MoS_2 is atomically thin, upon interaction with a target biomolecule, its whole thickness is affected, thus a higher sensitivity can be achieved. Another fascinating aspect of MoS_2 layers is the sensing abilities in the presence of particular sharp edge structures with feasible molybdenum and sulphur edges. Moreover, this powerful material also proved to have a great surface-area-to-volume ratio, high carrier mobility and low noise level (D. Zhang et al., 2016). Prior to that, the utilization of MoS_2 thin layer is essential to be functionalized the surface devices with the specific bio-(Kalantar-Zadeh and Ou, 2016). Furthermore, few layers/ultrathin of MoS_2 flakes as a Field Effect Transistor (FET) resulting in low-contact resistance (~0.8 kΩ μm) (Kappera et al., 2014; Liu et al., 2013b). In fact, a good edge contact between the metal contact to each MoS_2 layer edge promised a high ON current (24 μA/μm for 5 nmMoS2) even without doping at the source and drain (Liu et al., 2013a). Edge contacts are essential that allows an efficient process of electron injection into the MoS_2 layer, providing better mobility for the high-performance digital circuit.

Several label-based and label-free biosensor detections based on MoS_2 thin film have been developed. For label-free sensing, MoS_2-based Field-effect Transistor (FET) (Lee et al., 2015; Sarkar et al., 2014), MoS_2-based Screen-Printed-Electrode (SPE) (Kukkar et al., 2016) and MoS_2-based Modified Glassy Carbon Electrode (GCE)(Gan et al., 2018) while for label-based such as photoluminescence (Wang and Ni, 2014), fluorescence-based (Ha et al., 2014), and colorimetric (Mehrotra, 2016), have been demonstrated (Fig. 2). Fig. 2 (A to G) illustrate different detection mechanisms used in biosensor developments, i.e. calorimetric biosensor, electrochemiluminescence biosensor, field-effect-transistor (FET), glassy carbon electrode (GCE), the screen-printed electrode (SPE), electrochemical biosensor, and fluorescent based biosensor, respectively. The inset 2 (C) i) and ii) shows the transducer's modification together with the immobilization strategy on the sensing surface.

Here, our aim is to critically summarize the state-of-the-art progress on ultrathin 2D MoS_2, in particular emphasizes the recent advances on the label-free bio-sensing approach. We start with the discussion on the advantages of MoS_2 in relation to their composition and structures. Next, various synthesization methods for the preparation of ultra-thin 2D MoS_2 are described and comment on their advantages and limitations with inclusive of the characterization technique. Then, we describe the latest trend in label-free biosensing, utilizing MoS_2 as the transducing materials. Finally, we conclude on the current progress with personal insights on the challenges and outlooks in this promising field.

1.1. Synthetization of molybdenum disulfide (MoS_2)

Various methods have been demonstrated to obtain the monolayer of MoS_2 (Bhimanapati et al., 2015; Gupta et al., 2015; Liu and Xiang, 2017; Wang et al., 2017). As such, it is always promising to find the right technique suitable for different applications. This includes the mechanical exfoliation (Krishnamoorthy et al., 2016), liquid exfoliation (Coleman et al., 2011), chemical method (Lee et al., 2015), chemical vapour deposition (J. Lee et al., 2015), hydrothermal or solvothermal

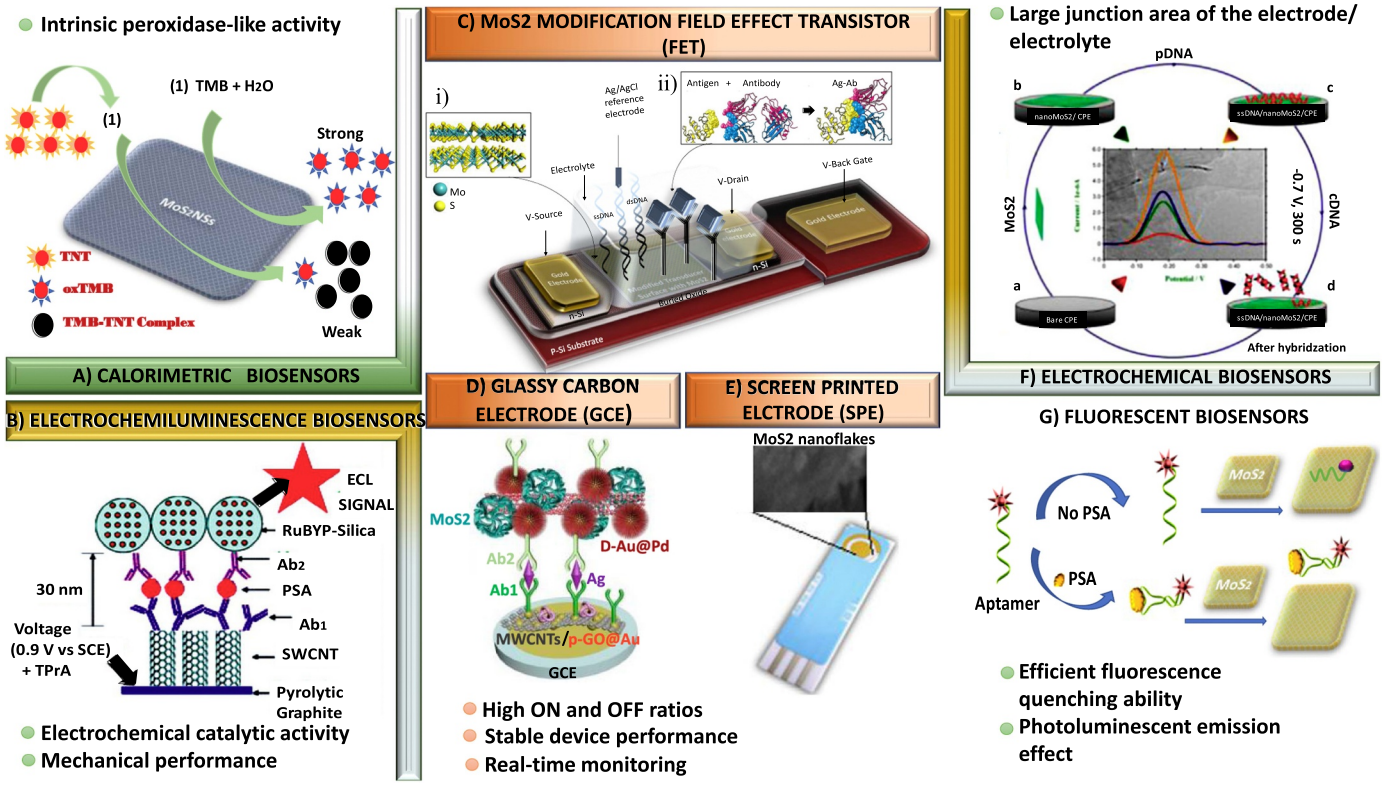

Fig. 2. (a) Calorimetric biosensor; (b) Electrochemiluminescence biosensor; (c) Typical schematic design for 4-electrodes MoS_2-based FET biosensor device, designed with source and drain contacts (to allow for the electrons to flow, creating the conducting channel), Ag/AgCl reference electrode (to supply bias to the electrolyte), back-gate terminal (for ambipolar switching conduction), dielectric layer covering the MoS_2 layer (not shown in figure), modified transducer surface with MoS_2 (linker i.e. (3-aminopropyl)triethoxysilane (APTES)/glutaradehyde (GA), Antibody/Probe i.e. Ab-CRP, Antigen/Target i.e. CRP). C) (i) 2D MoS_2 automatically layered pattern. (ii) Illustration for antigen/target and antibody/probe at before and after successfully binding; d) Glassy carbon electrode (GCE); e) Screen printed electrode (SPE); f) Electrochemical biosensor; G) Fluorescent biosensor.

method (Tan et al., 2017), and epitaxial growth method, which can be categorized into either top-down or bottom-up methods. The top-down methods covered delayering of adjacent layers into single or few layers, which includes the mechanical, liquid exfoliation, and chemical methods (Tan et al., 2017; Taniselass et al., 2019). As previously mentioned, for MoS_2, each monolayer made up of three atomic layers, in which a Mo is sandwiched between two S atoms. The monolayer is stack together through the weak van der Walls interaction. These stacked layers are easy to be broken their weak interaction into single or several layers by exfoliation methods. While, the bottom-up can be achieved by synthesizing nanomaterials with their corresponding pre-cursors, the methods include chemical vapour deposition and hydro-thermal or solvothermal method (Tan et al., 2017). It involves the chemical reaction of certain pre-cursor to grow the materials on the substrate. More discussion on the synthesis methods will be discussed in the next sub-chapter.

1.1.1. Mechanical exfoliation

The mechanical exfoliation/micromechanical cleavages, inherited from the first demonstration of 'scotch-tape' graphene, by Novoselov et al. (2004), which has been demonstrated to achieve the single layer MoS_2 materials. As shown in Fig. 3.1 (1) a) and b), the bulk graphene is adhered to the adhesive tape, repeatedly exfoliated followed by trans-ferring onto an appropriate substrate for the further application (Tan et al., 2017). The approach has been widely used and considered as a universal and conventional method to yield high 2D nanomaterials flakes, including MoS_2 (Tan et al., 2017). The processes are simple and do not require expensive equipment, capable to reduce the thickness of bulk material into thin nanosheets, hence produces the best quality and crystallinity of the 2D (Shan et al., 2018; H. Zhang et al., 2016). The original idea of this method was to weaken the van der Waals inter-action between the 2D nanomaterial layers. Thus, the peeling off the process of the layers will occur without rupturing the in-plane covalent bonds which result in a single layer (6.5 Å thick) (Radisavljevic et al., 2011; Tan et al., 2017). This approach does not involve either chemical or chemical reaction during the fabrication process, thus it can be ca-tegorized as a non-destructive method (Tan et al., 2017). Therefore, both exfoliated structures of single-layer and few-layer nanosheets yield almost flawless crystal qualities, expressed as a pristine layer from its layer bulk crystal. Despite this fact, this technique is time-consuming and lead to the low production, which is not advisable for high yield, large-scale, and various devices (Ma et al., 2018; Wang et al., 2017). In addition, the existence of uncontrolled sizes is still appear on the sub-strate due to this impractical approach, which has to be manually op-erated (Wang et al., 2017). Fig. 3.1 (1) b) show the monolayer graphene nanoflakes, which were prepared by standard Scotch-tape exfoliation method and Scotch-tape modified method. The surface treatment is demonstrated to improve the flake size and uniformity. The modifica-tion is started with oxygen plasma cleaning on the surface. Next, con-tact with the graphite-loaded tape, followed by annealing, cooling, and peel off. As a result, the monolayer flakes are expanding from 20 μm^2 × 20 μm^2 to ~500 μm^2 × 350 μm^2 after the treatment. Thus, the trans-formation of flake size is more than 400 times larger Fig. 3.1 (1) c) to e). In the nutshell, they have concluded that the modified Scotch-tape method is an efficient way to collect large-area flakes as compared to standard Scotch-tape method. In another study, the heat treatment during the exfoliation process and Au evaporation on the substrates have been introduced to improve the uniformity sizes (Tan et al., 2017).

In another approach, the mechanical exfoliation has been expanded to ball milling via mechanical shock forces by Krishnamoorthy et al.

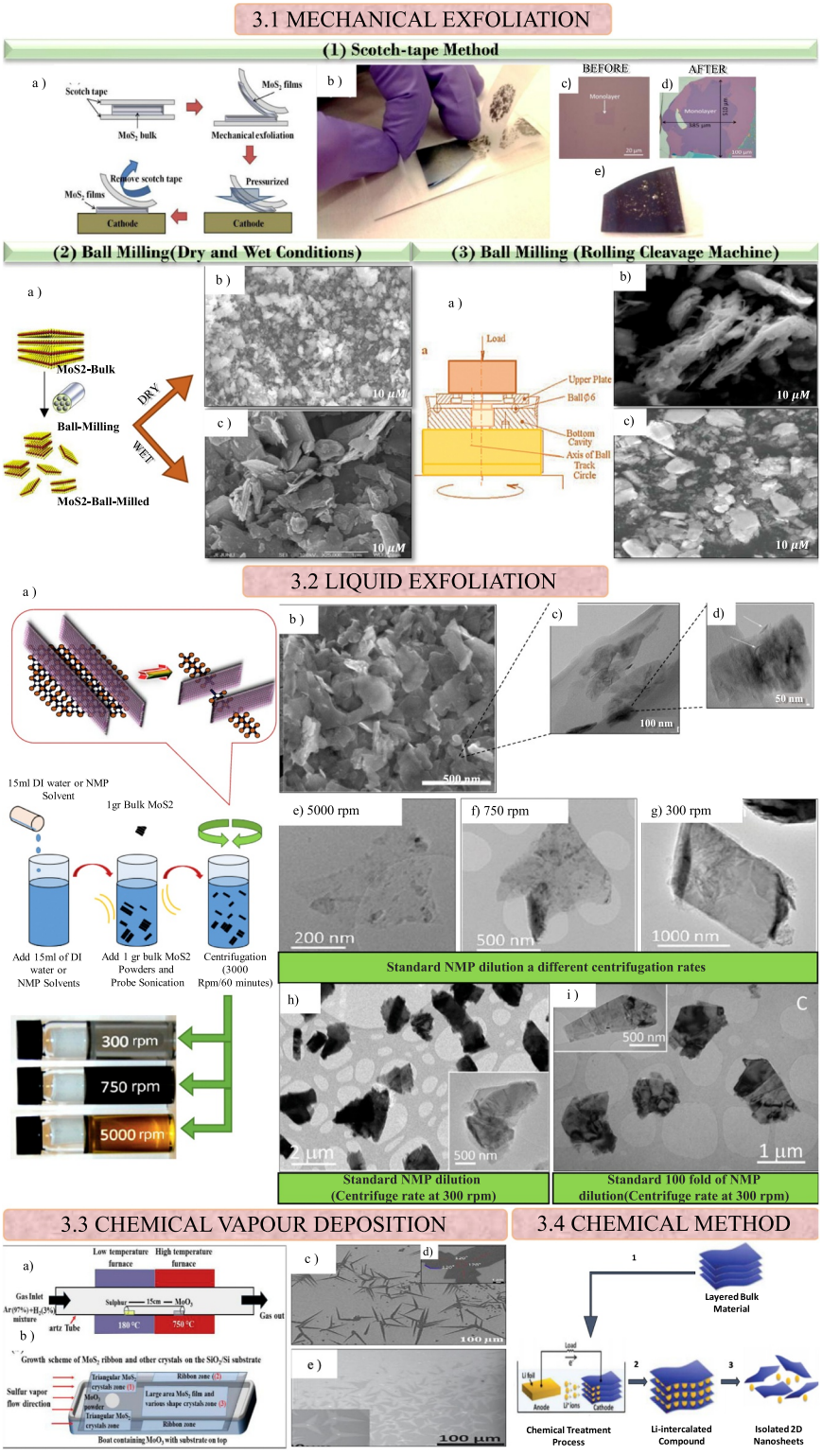

Fig. 3. 3.1 Mechanical Exfoliation: (1) Scotch-tape method, (a) Basic illustration of graphene synthesization by using Scotch-tape method, (b) manual peel-off process by hand, (c) transferring the exfoliated graphene onto the substrate, (d) and (e) before and after modification treatment modification treatment (Huang et al., 2015). Copyright 2015 American Chemical Society. (2) Ball milling using dry and wet methods, (a) Basic illustration of MoS_2 synthesization by using ball milling method (b) natural bulk MoS_2 turns to the sub-micrometer size of flakes after milling process. (Ambrosi et al., 2015). Copyright Elsevier B. V. (c) ball mill assisted exfoliated few layered MoS_2 at low magnification (Krishnamoorthy et al., 2016). Copyright 2016 Elsevier B. V. (3) Ball milling using rolling cleavage machine method. (a) An illustration of MoS_2 synthesization using rolling cleavage machine, (b) SEM images of MoS_2 particles after rolling cleavage during 3.5 h (c) MoS_2 thin platelets is less 15 nm. (Wiśniewska-Weinert, 2013). Copyright 2013 Elsevier B. V. 3.2 Liquid Exfoliation: (a) The schematic illustration of the MoS_2 sonication-induced exfoliation (b) SEM image of exfoliated MoS_2 flakes (c) and (d) TEM images of MoS_2 nanosheets by using pure water(e), f), and (g) Exfoliation of MoS_2 flakes at different centrifugation rate, 5000 rpm, 750 rpm, and 300 rpm by using NMP solution (45 min, 7.6 mg/mL) (h) Exfoliation of MoS_2 flakes at 300 rpm, with no additional NMP dilution and (i) with additional NMP dilution (O'Neill et al., 2012; Ma et al., 2018). Copyright 2018 Elsevier B. V. Copyright 2012 American Chemical Society. 3.3 Chemical Vapour Deposition (a) Schematic illustration of MoS_2 ribbon synthesization using CVD method (b) Different shapes of MoS_2ribbon/crystals growing on SiO2/Si substrate after synthesization. FE-SEM images of (c) Synthesized MoS_2 ribbons performing the individual and various branched structures. Inset (d) Higher resolution image at the center zone of the Y-shape ribbon pattern, produce the growth three arms at 120° surround the center zone (Mahyavanshi et al., 2017). Copyright 2017 Elsevier B.V. (e) Growth of MoS_2 star-shaped sheet layers on SiO2/Si substrate (pre-treated with rGO) by using Optical microscopic characterization (Lee et al., 2012). Copyright 2012 John Wiley & Sons, Inc. 3.4 Electrochemical lithiation steps for 2-dimensional nanosheets fabrication, from the layered bulk material until the isolation of 2D nanosheets (Zeng et al., 2011). Copyright 2011 John Wiley & Sons, Inc.

(2016) and low energy ball milling using the rolling cleavage machine Wiśniewska-Weinert et al. (2013), as illustrated in Fig. 3.1 (2) a) and (3) a), respectively. Krishnamoorthy et al. (2016) demonstrated the aforementioned approach of ball milling via the mechanical shock forces (under wet condition). The N-methylpyrrolidone has been employed as an exfoliation agent to peel-off the MoS_2 nanosheets. The dispersion of bulk MoS_2 was extracted and allowed the ball milling by using tungsten carbide balls and tungsten carbide bowls for 48 h of the period (Krishnamoorthy et al., 2016). For low energy ball milling, Wiśniewska-Weinert et al. (2013) has demonstrated this technique by using the rolling cleavage machine. The process allowing the balls to roll and slide, which are located in the track circle. As compared to the ball milling under wet condition, this method produces stable synthesization and faster processing time with improving quantity and quality of nanosheets, where the machine can be well controlled by the rotation speed (Wiśniewska-Weinert, 2013). Fig. 3.1 (2) b) c) and (3) b) c), further it shows the nanosheets morphology involving, ball milling (dry and wet), and ball milling using the rolling cleavage machine.

In Fig. 3.1 (2) b), Ambrosi et al. (2015) have reported the grains were successfully synthesized into sub-micrometer of flakes by using dry ball milling process. In a different method, the surface morphology of ball milled MoS_2 under the wet condition was analysed using FE-SEM [Fig. 3.1 (2) c)], proving the existence of MoS_2 sheet-like morphology with varies in lateral thickness and sizes (Krishnamoorthy et al., 2016). Krishnamoorthy et al. (2016) proven the existence of sheets with less thickness and the lateral size within the range of 700–200 nm via ball milling under the wet condition (NMP agent) (Krishnamoorthy et al., 2016). On the other hand, they have proved that wet exfoliation strategy enhances the production of few-layered MoS_2 nanosheets through the mechano-chemical delamination from its bulk (Krishnamoorthy et al., 2016) as compared to the dry exfoliation strategy. Next mechanical exfoliation ball milling approach using the rolling cleavage machine, Fig. 3.1 (3) a) shows an illustration of a rolling cleavage machine used to yield a high quality of MoS_2 nanosheets by Wiśniewska-Weinert et al. (2013). Fig. 3.1 (3) b) captured thin flakes of MoS_2 by the combined methods of shear and normal stress at the device trailing edge. They have reported the presence of nanoflakes of 200–500 nm by using SEM [Fig. 3.1 (3) c)]. They claimed that the transparent flakes captured are probably lesser than 15 nm of platelets thickness. Therefore, this method has claimed by (Wiśniewska-Weinert, 2013), to be a strong potential of MoS_2 with a large scale manufacturing as solid lubricants.

1.1.2. Liquid exfoliation

Liquid exfoliation is a method which produces 2D flakes dispersed in a liquid medium (Schwierz et al., 2015). Coleman's group was the first team who developed this simple and facile method, proposing the synthesization of graphite into graphene (Hernandez et al., 2008). Very recently, Majd et al. (2018) demonstrated MoS_2 synthesization through the liquid exfoliation techniques which involve chemical approaches, such as mechanical force-assisted liquid exfoliation and ion intercalation-assisted liquid exfoliation (Ghasemi and Mohajerzadeh, 2016; Li and Zhu, 2015). Basically, mechanical force-assisted liquid exfoliation can be categorized into two parts, which are sonication-assisted liquid exfoliation and shear force-assisted liquid exfoliation. In ion intercalation-assisted liquid exfoliation, the ion intercalation occurs when tiny guest atoms, such as lithium, is penetrating into the MoS_2 sandwich layers which weakening those interlayer interactions of MoS_2. Hence, it paves the way to the smooth exfoliation of flakes in aqueous solution.

For mechanical force-assisted liquid exfoliation, the sonication-assisted exfoliation is the most common method. The sonication produces a high-yield of the dispersion quality of few-layered MoS_2. (Ghasemi and Mohajerzadeh, 2016; Majd et al., 2018) have completed their MoS_2 liquid exfoliation technique based on a high-power sonication, aided by materials that strengthen the physical surface adhesion on stratified MoS_2 (Ghasemi and Mohajerzadeh, 2016). The group reported that this method has been immensely utilized due to the low-cost mass production, simplicity and relatively high output (Ma et al., 2018). Fig. 3.2 a) shows the schematic illustration process to prepare the MoS_2 fragment nanosheets and the basic understanding of how the chemical bond fragmentations occur from the peeling operation (sonication induced exfoliation). The sonication approach can be assisted either by pure water (Ma et al., 2018) or N-Methyl-2-pyrrolidone (NMP) or dimethylformamide (DMF) solvents (Ghasemi and Mohajerzadeh, 2016; Wang et al., 2013).

Direct exfoliation of MoS_2 nanosheets using pure water has been demonstrated by Ma et al. (2018). In this case, water was found to be a very useful dispersible solvent for MoS_2 nanosheets (Yu et al., 2018) as compared to alcohol solvent. In the experimental work, the bulk MoS_2 powder was mixed with deionized water and the resultant dispersion was sonicated. Next, the mixed solution was kept fixed to allow the sedimentation to occur and the upper solution was centrifuged to remove the thick flakes. Tan et al. (2017) discussed that simply heating the pure water promising stable exfoliated nanosheets of 2D materials, inclusive of MoS_2. Finally, the supernatant was thoroughly extracted in order to collect MoS_2 aqueous dispersions. Under Scanning Electron Microscopy (SEM), Fig. 3.2 b) shows the exfoliated nanosheets of MoS_2, which has been exfoliated from micrometer to nanometer range of flake size. This achievement proved a successful synthesization of bulk MoS_2 particles and substantially fragmented. Fig. 3.2 c) and d) are confirmation of few-layer nanosheets and multilayer nanosheets localized at different spots. This phenomenon elucidates that the results are a mixture of few-layer and multilayer patterns.

Other studies using NMP (O'Neill et al., 2012) and DMF (Wang et al., 2013) contribute to excellent electrocatalytic performance in other related applications (Wang et al., 2013). These aforementioned techniques were used in extracting the 2D MoS_2 suspensions in organic aqueous solvents adaptable for biosensing operations (Majd et al., 2018). The size of the MoS_2 nanosheets decreased at longer sonication times due to the sonication induced scission, shown in Fig. 3.2 e) to g) (O'Neill et al., 2012). The controlled centrifugation process is important, since the process caused the MoS_2 nanosheets flakes to be lying on the mixed-solvent top surface. It allows the enhancement of edges as well as prevent the nanosheets from aggregation or assemble. As a result, the dissimilar contrast of the nanosheets can distinguish the layers (either thick or thin). The structure of hexagonal symmetry prescribes that MoS_2 crystal structure is not spoiled or damaged during the exfoliation (Ma et al., 2018). For different NMP concentration, the flakes were marginally thinner when reducing the concentration by 100 folds as demonstrated at 300 rpm [Fig. 3.2 h) and i)] (O'Neill et al., 2012). Similar results were observed by using DMF solvent (Wang et al., 2013). In addition to those factors, the power and temperature of sonication also impact the desired nanosheets (Schwierz et al., 2015; Tan et al., 2017).

1.1.3. Vapour/gas chemical deposition

Scalable production and yielding a large number of ultrathin flakes are truly significant for high advance applications (Sun et al., 2012; Tan et al., 2017). Hence, the development of CVD technique has been greatly implemented to overcome this issue. The first utilization of chemical vapour deposition (CVD) method in the industry was dated back in 1897 by de Lodyguine, for lamp application (Guine, 1897). Extended to 2D nanomaterials, Tan et al. (2017) reported that Somani et al. (2006) were the first inventors who demonstrated the CVD technique in the year 2006, proving the growth of a single or few layers toward graphene. Six years later, in the year 2012, the synthesization technology has been further investigated using MoS_2 material. Thereby, Chang et al. (2012) was the first group who demonstrated few-layer MoS_2 nanosheets growth using CVD method This method can be attributed to a growing process of the ultrathin layer, either organic or inorganic precursor (e. g. solid, liquid or gaseous) of 2D MoS_2 and continue with series of annealing as well as sulfurization steps (Bonaccorso et al., 2012; Tan et al., 2017) aiming for less lateral thickness and a high interlayer distance of MoS_2 flakes for viable applications (Amini et al., 2017). This MoS_2 synthesization resulting in a uniform and high-quality layers, high purity, and limited defects of 2D nanomaterials on substrates which can hugely avoid the presence of interfacial contamination formation during layer by layer process (Li and Zhu, 2015; Mahyavanshi et al., 2017). More importantly, the crystallinity and the grade substrate are essential to achieving a smooth deposition process. In addition to MoS_2, several ultrathin 2D nanosheets of TMDs was grown using the CVD method, including tungsten disulfide (WS_2), and molybdenum diselenide (MoSe2) which has been extensively used in nanomaterial biosensor technology development (Tan et al., 2017), as well as in optoelectronics and electronic devices (Chhowalla et al., 2016; Tan et al., 2017).

In order to apply CVD synthesis method, sulphur and molybdenum trioxide (MoO_3) precursors were laid in a small quartz tube in the first place [Fig. 3.3 a) and b)]. They observed that sulphur and MoO3 vapour exposure are affecting the shape of MoS_2 crystals. They pointed-out, it is

significant for implementing better channeling of sulphur vapour, to make it reacts with the evaporated MoO_3. It needs to adjust in the center area of the boat, in order to allow the traveling of gas with sulphur vapour (Mahyavanshi et al., 2017), need to leave a small gap distance between tail and head in the prepared boat. After that, both MoO_3 and sulphur heating areas began to grow independently. During this process, evaporation for MoO_3 precursor is smooth. Unfortunately, an evaporation process for the sulphur is slow and took some times, caused by poor dissipation of heat at a low temperature of the CVD machine. A study has proved that controlling the flow rate may evade the inconsistently and unmanageable reaction between the MoO3 and sulphur precursors. Mahyavanshi et al. (2017) has demonstrated their project by optimizing the gas mixture flow which is hydrogen and argon at 3% and 97%, respectively, carrying the evaporated sulphur. The MoS_2 ribbon shape was growing at the outside of the substrate's area. In fact, it was extended from the substrate holder boat. The evaporated MoO_3 diffusion is pretty less to the outside of the boat. Therefore, this phenomenon has given opportunities to sulphur, to grow abundantly in the outside edges area of the extended substrate. Considering this special approach, it is capable to grow MoS_2 ribbon and branch in various domain shapes, such as unidirectional, bi-directional (V-shaped), tri-directional (Y-shaped) (Lee et al., 2012; Mahyavanshi et al., 2017), and sharp triangular corners (Chen et al., 2018). For branch structure, individual and variety structures were obtained, 5–10 μm (width) and 50–100 μm (length), respectively [Fig. 3.3 c)]. Fig. 3.3. d) shows a higher resolution image of the Y-shape ribbon pattern with the growth of 120° three arms at the center [Fig. 3.3 d)]

In contrast to the previous study, Chen et al. (2018) has transferred as grown monolayer MoS_2 on a sapphire substrate. Two techniques of CVD have been proposed including atmospheric pressure chemical vapour deposition (APCVD) and low-pressure chemical vapour deposition (LPCVD). In this experiment, the isolated monolayer MoS_2 crystals have been immersed in PBS solution. As a result, an arrowhead with grain boundaries region and localized holes of point defects appear. In this case, the few parameters such as pH level (7.4), temperature (75 °C), time (49 days), concentration (60 mL of 1.0 M), and the type of ions in the PBS solution are being considered to completely dissolve the polycrystalline MoS_2 monolayer (grain size approximately 200 nm) (Chen et al., 2018).

Alternatively, Lee et al. (2012) has reported that pre-treated SiO2/Si substrate with the reduced graphene oxide (rGO) may promote the layer growth, highly reproducible for MoS_2 layers. They reported the homogenous thickness layer can be produced by applying this alternative treatment. Fig. 3.3 e) shows the growing of MoS_2 with star-shape, was started from the seeds, where its width has downsized from the nucleation point (white dot) toward the end point of the MoS_2 ribbon. A continuous film of MoS_2 (lateral size is up to 2 mm) can be formed when most of the star-shaped MoS_2 are merged.

The monolayer MoS_2 film is successfully formed between without pre-treated rGO (Mahyavanshi et al., 2017) and pre-treated rGO (Lee et al., 2012), with a thickness of 0.7 nm and 0.72 nm, respectively. However, researchers are still facing several challenges in order to proceed with the CVD method. One of the problems is the substrates which have been deposited with ultrathin 2D materials need to be shifted to other substrates (Tan et al., 2017). Additional manual work needs to be considered later on. Besides, it requires an inert atmosphere environment and a high temperature to allow the growth of MoS_2 sheets. Solution-based methods are much cheaper as compared to the CVD technique. Moreover, the difficulty to control the number of MoS_2 nanolayers and the phases remain as a challenge until today (Chhowalla et al., 2016)

1.1.4. Hydrothermal reaction

The hydrothermal method also known as the solvothermal method is a process to crystallize the substance from an organic or aqueous solution (Gupta et al., 2015; Tan et al., 2017). This wet-chemical synthesis has been invented to produce high yield, controllable size and uniform thickness of 2D nanomaterial layers (Tan et al., 2017). The process was operating at a high vapour pressure-temperature to ensure best growth phase stability and solubility as well as producing great catalytic activity for biosensor (Gupta et al., 2015; Tan et al., 2017).

Gupta et al. (2015) synthesized these 2D materials by implementing a chemical reaction process between sulphur and/or selenium and ammonium molybdate in hydrazine monohydrate solution at the temperature of 150 °C to 180 °C for 48 h. As a result, no restacking tendencies produced in both of the monolayer samples, with no usage of the surfactant. Recently, Zhu et al. (2017) has demonstrated a two-step hydrothermal technique to synthesize three-dimensional flower-like MoS_2/TiO2 nanohybrid, which is constructed with MoS_2 nanosheets as well as TiO2 nanoparticles. They utilized a two-step hydrothermal method, which is a process of MoO2/TiO2 precursor formation and sequent valcunization to the MoS_2/TiO_2. They obtained the homogenous layer from the dispersion of TiO_2 nanoparticles on the MoS_2 nanosheets and demonstrated the high reversible capacity of 801 mA h g^{-1} at a current density of 100 mA g^{-1} after 50 cycles. The two-step hydrothermal MoS_2/TiO_2 nanohybrid has promised good structure stability as compared to bare MoS_2. This modification is also capable to shorten the distance transportation for ions across the surface (Zhu et al., 2017).

Nevertheless, since the reactions happened in a sealed autoclave, there are some difficulties to observe the growth mechanism (Tan et al., 2017). Thus, it poses a great challenge to design the experiment for other material operation. Furthermore, the experimental conditions, including solvent systems, temperature, and precursor concentrations, are quite sensitive (Gan et al., 2017; Tan et al., 2017), need a skillful person to conduct the experiment. Challenges such as i) selection and availability of chalcogen reagents and metal; ii) understanding how to permit lateral growth while truncate vertical growth; iii) control over metal oxidation states; also need to be considered by using this method.

1.1.5. Chemical Methods

In essence, chemical methods are on the basis of ion intercalation, (e.g. $SO4^{-2}$ and Li^{+}) (Gan et al., 2017; Wang et al., 2017). Similar to other techniques, the chemical method also promising large yielding of MoS_2 monolayer (Liu et al., 2014). As shown in Fig. 3.4 a), Liu et al. (2014) has developed an exfoliation method and electrochemical Li-intercalation to extract the MoS_2 nanosheets. The process started when the MoS_2 layered bulk material was incorporated as a cathode (test cell) and lithium foil as an anode to provide lithium ions. After the lithium insertion was completed, the intercalated compound was washed with acetone (intercalated compound: e.g. Lix MoS_2). The purpose was to remove the residual electrolyte from the previous process. Next, ultrasonicated in ethanol or water for the exfoliation and isolation of 2D nanosheets (Zeng et al., 2011). An interlayer dimensions were extended when the lithium ions were successfully infused into the bulk material interlayer spaces, hence weakens the van der Waals interaction from one layer to another layer. Liu et al. (2014) has confirmed that 5–50 μm lateral size of MoS_2 nanosheets can be obtained by chemical exfoliation methods. In comparison, they have claimed that this MoS_2 nanosheets lateral size were much larger by using chemical exfoliated rather than liquid-phase exfoliated.

Nevertheless, this technique is time-consuming and involved harsh chemical treatments, which requires the need for an inert environment (Gan et al., 2017; O'Neill et al., 2012). This method leads to the structural deformations and defects on the synthesized MoS_2 layers (Gan et al., 2017; Wang et al., 2017)

1.1.6. Pulse laser deposition (PLD)

Pulse laser Deposition (PLD) is a technique to grow controllable nanoflakes by using a different number of laser pulses (Pradhan and Sharma, 2018). The exciting lasers were used to deposit thin film 2D nanomaterial, inclusive of MoS_2, under slower growth kinetic on 'c'

Table 1
Detection methods applicable to the development of device based-MoS2 for detection of various biomarkers antigen.

Detection Method	Device Structure	Target	Fabrication Hierarchy	Concentration	Limit of Detection	Assay Principle	References
MoS_2 on FET	FET	IgG/Anti-IgG	Si/SiO2/Ti-Au metal contact pad/ MoS_2/APTES (amine group)	10 pg/mL to 100 μg/mL	100 μg/mL	IV measurement	(Lee et al., 2015)
MoS_2 on FET	FET	PSA/Anti-PSA	Si/SiO2/Ti-Au metal contact pad/ MoS_2/APTES (amine group)	100 μg/mL	Ipg/mL	IV measurement	(Lee et al., 2015)
SL- MoS_2 fluorescence detection electrochemical lithium intercalation	FRET aptasensor	pLDH	MoS_2/pLDH aptamer/pLDH protein/Aptamer protein complex Incubation: 10 mins	8 μg/mL	550 pM	Fluorescence measurement	(Kenry et al., 2016)
Ultrasensitive sandwich-type electrochemical immunosensor	GCE	HBs/Anti-HBs	GCE/ MoS_2 @Cu2O-Pt NPs/APTES (amine group)/Ab1/HBs Antigen/ MoS_2 @Cu2O-Pt NPs/ Ab2)	0.5 pg/mL to 200 ng/mL	0.25 pg/mL	Amperometric	(Li et al., 2018)
Aptasensor by ATP and thrombine aptamer (AUNPs- MoS_2)	GCE	Thrombin and ATP (detection agent)	GCE/AuNPs- MoS_2/Aptamer, μM TBA, 1.0 μMds-APTA,10 mM Tris-HCL,0.1 mM TCEP)	ATP: 1 nm to 10 mm Thrombin: 0.01 nm to 10 μm	ATP: 0.74 nm Thrombin: 0.0012 nm	NPV, CV, EIS, SWV	(Su et al., 2016)
Glassy carbon electrode modified with MoS_2 nanosheets and poly (3,4-ethylene dioxythiophene) (PEDOT)	GCE	Ascorbic acid (AA), dopamine (DA) and uric acid (UA)	GCE/Ag/AgCl electrodes/ MoS_2/PEDOT	AA: 0.2 mM to 1.2 nM DA: 1.0–80 μM UA: 4.0–30 μM	AA: 5.83 μM DA: 0.52 μM UA: 0.95 μM	CV/DPV	(Deng et al., 2016)
MoS_2-PABSA via simple electropolymerization	GCE	TNT	GCE/conjugated MoS_2-PABSA/	1 mg/mL	0.004 ppb	CV	(Yang et al., 2016)
CTAB MoS_2 on microfluidics electrode	ITO microfluidic chip	s.typhimurium/Anti-s.typhimurium	ITO/CTAB/ MoS_2 NS/PDMS microfluidic/APTES (amine group)	NA	1.56 CFUm/L	EIS	(Singh et al., 2018)
MoS_2/TiO2/SiNW for SALDI-MS detection	LDI-MS	DNA	LDI-MS Mass /Si/Tio2/SiNW/ MoS_2/1H, 1H, 2H, 2H-per fluoreodecanethiol (PEDT)/glutathione or glucose	10 nmol/ μL	Gluthathione: NA Glucose: 1pmol/ μL	Mass spectrometry analysis	(Hamdi et al., 2017)
MoS_2 modified SPE wit presence $Fe^{3+/}Fe^{2+}$redox probe	SPE	BSA/Anti-BSA	SPEs/ MoS_2 redox solution 5 mM $K_3Fe(CN)_6$ + $K_4Fe(CN)_6{\cdot}3H_2O$ (in 0.1 M PBS) Incubation: 20 mins	0.01 ng/mL to 10 ng/mL	6 pg/mL	CV	(Kukkar et al., 2016)
Bio solution-gated MoS_2 FET/DNA hybridization	FET	DNA	Si/SiO2/ MoS_2/Au-Cr drain-source electrodes/ Al_2O_3 /direct immobalized/target DNA/PDMS well/DNA Probe single-stranded – probe DNA (5'-CTG TCT TGA AA TGA GTI − 3'), complementary target DNA (5'AAC TCA TGT TCA AGA Cag − 3'), noncomplementary DNA (5'- AAC TCA TGA TCA AGA CAG − 3')	NA	10fM	IV measurement	(D.-W.Lee et al., 2015)
MoS_2 nanosheet modified with thionine and gold nanoparticle	GCE	mir − 21	MoS_2-Thi-AuNPs/GCE/probe DNA/MCH/mir − 21 Incubate: 25°C at 16 h	1 pM to 10 nM	0.26 pM	SWV/EIS	(D. Zhu et al., 2017)
Label-free and directly hybridization of MoS_2	FET	miRNA − 155	Si/SiO2/Ti-Au source-drain metal pad/ MoS_2/ miRNA conjugate/probe miRNA − 155/	0.1 fm to 10 nm	0.03 fm	IV measurement	(Majd et al., 2018a)
MoS_2 nanoparticles for electrochemical detection of H2O2	GCE	Raw 264.7 cells	MoS_2/GCE/Nafion	2 x 10^6 cells into 20 mL of PBS	2.5 nM	CV, Amperometric	(Wang et al., 2013)
Cu2 + -DNA/MoS_2 hybrid structure	FET	dexorubicin	Si /SiO2/ MoS_2/Cu^{2+}-DNA	10^{-4} μM to 50^{-4} μM	Sensitivity:1.7 × 10^3 A/A	IV measurement	(Park et al., 2016)
MoS2-graphene for vitro detection	Au-PCB	Parathyroid hormone (HRP)	((ALP)/HRP)-IgG/PTH/MoS_2-graphene	1–50 pg/mL	5 ng/mL	CV, EIS	(Kim et al., 2016)
MoS_2-wearable sweat biosensor detecting low-volume perspired human sweat	Vertically aligned electrode stack	Cortisol	PA membrane /MoS_2/palladiumvertically alligned electrode stack/ MoS2/ PA membrane/ DSP linker	1 ng/mL to 500 ng/mL	1 ng/mL	EIS	(Kinnamon et al., 2017)
3D Cu nano-flowers/layered MoS_2 composite	GCE	Glucose and H_2O_2	CuNFs-MoS_2/GCE (immersed with $Cu(NO_3)_2$ solution)	H_2O_2: 0.04– 1.88 μM and 1.88–35.6 μM Glucose: 1–20 μM and 20–70 μM	H_2O_2: 0.021 μM Glucose: 0.32 μM	EIS/CV	(Lin et al., 2016)
Paper-based-MoS2 for rapid malaria diagnosis	FRET aptasensor	pLDH	Printer paper/MoS2/aptamer Papers tested: lens paper, coffee filter, printer paper, Advantec, Whatman	100 nM	550 pM	Fluorescence measurement	(Geldert and Lim, 2017)

(*continued on next page*)

Table 1 (*continued*)

Detection Method	Device Structure	Target	Fabrication Hierarchy	Concentration	Limit of Detection	Assay Principle	References
Structuring AuNPs-MoS2 for electrochemical glucose biosensors	GE	Glucose oxide	Gold electrode/MoS2/ AuNPs/glucose oxide	0.25–13.2 mM	0.042 mM	CV, EIS, Amperometric	(Parlak et al., 2017)
Polyaniline-MoS2 Hybrid Nanostructures for Cancer Biomarker Detection	ITO electrodes	pDNA	pDNA/PANI-MoS2/ITO	10^{-6} M to 10^{-17} M	3×10^{-18} M	CV, EIS	(Soni et al., 2018)
Functionalized MoS2 hybridized with polypyrrole nanotubes	GCE	alpha fetoprotein	Pt NDs/PDDA/MoS2 @PPy NTs	50 fg/mL to 50 ng/mL	17 fg/mL	CV, EIS	(Pei et al., 2019)
MoS2-peptides for sensitive detection of Caspace – 3 activity	FRET	Caspace – 3	MoS2 @PDA-PEG-Peptide, MPPP/FAM-labelled substrate	2 ng/mL to 360 ng/mL	0.33 ng/mL	Fluoresence recovery	(Li et al., 2019)
Photoelectrochemical platform based on polyaniline-nanoMoS2 composites	GE	glutathione	PANI/nanoMoS2/GE	1.0×10^{-10} mol/L to 1.0×10^{-4} mol/L	3.1×10^{-11} mol/L	Photocurrent response	(Hun et al., 2018)
Highly sensitive determination based on thin-layered MoS2/polyaniline nanocomposite	CPE	chloramphenicol	MoS2/PANI/CPE	1.0×10^{-7} mol/L to 1.0×10^{-4} mol/L	6.9×10^{8} mol/L	DPV	(Yang et al., 2015)
Development of an effective electrochemical platform using MoS2 - polyaniline nanocomposites	Pt electode	DNA	Pt/MoS2-polyaniline/ssDNA	NA	10^{-15} M	DPV, IV measurement	(Dutta et al., 2018)
Sandwich-type ELISA based on Ag/MoS2 @ Fe3O4 and an analogous ELISA method with total internal reflection microscopy	MGCE	carcinoem- bryonic antigen (CEA)	Ab2-Ag/MoS2 @Fe3O4/MGCE	0.0001 ng/mL to 20 ng/mL	0.03 pg/mL	DPV, EIS	(Wang et al., 2018)

Note: CTAB - cetyltrimethyl ammonium bromide, SL – single layer, MoS_2-PABSA - molybdenum disulfide-poly(m-aminobenzenesulfonic acid), SALDI-MS – surface-assisted laser desorption/ionization mass spectrometry, PDMS – polydimethylsiloxane, LDI – laser/desorption ionization, pLDH – plasmodium lactose dehydrogenase, TBA – thrombin binding aptamer, PEDOT - poly(3,4-ethylenedioxythiophene), NPV – normal pulse voltammetry, CV – cyclic voltammetry, EIS – electrochemical impedance spectroscopy, SWV – square wave voltammetry, DPV – differential pulse voltammetry, PA - porous polyamide, DSP - Dithiobis [succinimidyl propionate], GE – gold electrode, CPE – carbon paste electrode, PT - platinum electrode, ITO – indium tin oxide, MGCE – magnetic glassy carbon electrode.

plane sapphire (Sahu et al., 2017). This kind of treatment does not require any additional/special treatment, clear from any parasitic deposition, and more scalable on a larger substrate, in order to grow the monolayer MoS_2 which has some betterment over CVD.

By varying the deposition time with the duration of 14 s, 24 s, 30 s, and 6 min, (Pradhan and Sharma, 2018) have reported the growth of MoS_2 film; monolayer, bilayer, and trilayer, on SiO_2/Si substrate by using PLD. They analysed that the increase deposition time lead to the formation of unwanted distributed island formation. This can cause some degradation to the material crystallinity. Considering the time, 13 nm average size of nanocrystallites along with MoS_2 layered film was achieved at shortest deposition duration, 14 s. In addition, Sahu et al. (2017) reported that inducing strain through the substrate may enhance the growth mechanism of MoS_2 material via the PLD method. They witnessed that further stiffens through the substrate (significant Raman active modes; E12g and A1g) resulting in the decreasing of MoS_2 layer thickness. Specifically, maximum compressive strain (strain energy: 10 meV, 0.52%) for monolayer MoS_2, elevates the band gap to 1.73 eV from 1.68 eV, and drops with increasing the thickness of layers. Briefly, the process started with the sintering of MoS_2 pellets from pure MoS_2 powder, followed by applying pressure towards pellets via a hydraulic system. These MoS_2 pellets were utilized as a target in PLD. Next, they applied a high-power Nd: YAG laser to focus on MoS_2 target. In contrary, Zabinski et al. (1992) applied KrF excimer laser to be focusing on the target. From both demonstrations, the differences between Nd: YAG laser and KrF excimer laser are the types of substrate and the number of radiation wavelength; SiO_2/Si substrate (355 nm (Pradhan and Sharma, 2018) and stainless-steel substrate (248 nm) (Zabinski et al., 1992), respectively.

In summary, the MoS_2 sheets deposition reveals an epitaxial compression due to its adhesion to the SiO_2/Si substrate (Pradhan and Sharma, 2018). In PLD technique, stiffening of both Raman modes giving good impact to the increment of direct bandgap state (Sahu et al., 2017), hence, providing a high opportunity in the optoelectronic field and device fabrication.

2. Application of thin film molybdenum disulfide (MoS_2) biosensors

According to the International Union of Pure and Applied Chemistry (IUPAC), the biosensor is defined as devices to evaluate specific biochemical reaction via bio-receptors by electrical, thermal or optical signals (IUPAC, 2014). Likewise, Wang et al. (2014) defined the biosensor as a combination of biorecognition features with a transducer to create the interactions between the biorecognition element and the particular target to an output signal target. In fact, the fields of biosensors and bioelectronics are interrelated and according to (IUPAC, 2014), bioelectronics is the utilization of biomolecular concepts to microelectronics. Basically, there are two main types of biosensing strategies which are label-based and label-free detection method. Label-based is defined as any foreign molecule that is temporary or chemically conjugated to the molecule of interest and it relies on “labels” or “tags” to detect a selected analyte in specific properties (Sang et al., 2015; Syahir et al., 2015). In contrast, label-free is a technique that does not require labelling of the receptor or ligand to allow screening of analytes. Instead, this method utilizes molecular biophysical properties to monitor the activity of the molecule. Nevertheless, label-free biosensors presented in experimental procedure met the specifications in terms of high sensitivity and fast detection (Adzhri et al., 2016; Fathil et al., 2016), such as field-effect transistors (FETs). As compared to label-free detection methods, conventional label-based detection methods, for example, the enzyme-linked immunosorbent assay (ELISA) (Letchumanan et al., 2019; Wang et al., 2014), fluorescents biosensor, electrochemiluminescence biosensor, and calorimetric biosensor (Gan et al., 2017), consist drawbacks including complexity in sample processing, higher operational costs, lack of portability, and limited

applications in real-time monitoring (Wang et al., 2014). Thus, current label-free biosensors based on 2D MoS_2 become the main focus in the biosensor world. It can be categorized into several structures or architectures such as electrode-based devices (FET, GCE, SPE, IDE), electrodeless optical systems and reverse electroluminescent systems (Kalantar-Zadeh and Ou, 2016; Nordin et al., 2016). Table 1 displays detection methods applicable to the development of device based-MoS_2 for detection of various biomarkers antigen, inclusive of the label and label-free methods.

2.1. Label-based MoS_2 based biosensor

Recently, MoS_2-electrochemical biosensors are being implemented in the areas of environmental monitoring, healthcare, and food packaging (Mao et al., 2017). Secondly, MoS_2-fluorescence biosensors have been widely used for signal amplification which can improve the sensitivity of biosensor (Mao et al., 2017), especially in the detection of multiple target analytes (Gan et al., 2017). Thirdly, MoS_2-electrochemiluminescence biosensors are involving a light emission process in a redox reaction. This method has been reported, potentially enables high cell capture efficiency and enhance electron transfer kinetic (Kumar et al., 2015; Mao et al., 2017). Last but not least, MoS_2-calorimetric biosensors demonstrated with the peroxidase-like activity on 2D MoS_2 and have been reported to be applied in a real-life biological sample (Mao et al., 2017)

2.1.1. Bio-imaging

MoS_2 has been extensively used in fluorescence probe for bio-imaging applications. It possesses variant morphology which is suitable in the optical properties area (Barua, 2017). In this study, Wang et al. (2016) introduced MoS_2 quantum dot@polyaniline (MoS_2-QD@PANI) nanohybrids for the enhancement of photoaccoustic (PA) imaging/X-ray computed tomography (CT) and deliver the qualified radiotherapy (RT)/photothermal therapy (PTT) of tumour cells. Besides, imaging applications based MoS_2 also has been explored by Han et al. (2016) for the integration of multifunctions of photodynamic therapy (PDT), photothermal therapy (PTT), and up-conversion luminescence (UCL) imaging for antitumor enhancement efficiency. They reported that covalently grafted up-conversion nanoparticles (UCNPs) were prepared with chitosan functionalized MoS_2 (MoS_2-CS) and folic acid (FA). After that, the surface of MoS_2 was loaded with phthalocyanine (ZnPc) to form MoS_2-UCNPs-FA/ZnPc. Multimodal bioimaging for modern biomedical appliances based MoS_2 has been demonstrated by Liu et al. (2017). They designed a multifunctional composite of MoS_2 @Fe_3O_4-indocyanine green molecules (ICG)/platinum (Pt(IV) prodrugs). The Fe_3O_4 nanoparticles are covalently grafted with polyethylenimine (PEI) functionalized MoS_2 and loaded the MoS_2 @Fe_3O_4 surface with ICG and Pt (IV). This proposed nanocomposite has provided outstanding infrared thermal/magnetic resonance/photoacoustic trimodal bio-imaging impressively enhanced antitumor efficacy of combined photodynamic therapy, photothermal therapy, and chemotherapy triggered in cancer treatment and diagnosis.

2.1.2. Healthcare diagnosis

In this study Wang et al. (2016), ELISA method has been applied for carcinoembryonic antigen (CEA) detection by executed on glassy carbon electrode (MGCE). The structure Ab_2/Ag/MoS_2 @Fe_3O_4 was used as a label and total internal reflection fluorescence (TIRF) technique has been applied for the proposed method verification. DPV and EIS were applied for the detection of CEA and confirmation of successful fabrication of immunosensor, respectively. A linear response was obtained in the range of 0.0001 ng/mL to 20 ng/mL with a low detection limit as low as 0.03 pg/mL. These successful outputs revealed that the proposed method could provide a sensitive detection of CEA antigen. In summary, it provides a promising platform to detect the existence of any kind of tumour markers.

2.1.3. Environmental monitoring

Silver ions (Ag+) are capable to induce prominent toxic effects fungi, viruses, algae and bacteria. This heavy metal is dangerous which can critically affect the environment condition, especially for water resource. Fortunately, the biocompatible nature of MoS_2 allows monitoring of soluble silver ion (Ag+) ion in living *E. coli* (Wang and Mi, 2017). Therefore, Yang et al. (2015) has successfully designed a simple and facile MoS_2-based fluorescent nanoprobe for intracellular detection of both Ag+ ion in living E. coli cells and in aqueous solution. Sensitive and selective detection was greatly achieved by using rhodamine B isothiocyanate (RhoBS)-MoS_2 nanosheets via FRET. Highly sensitive detection of Ag+ (down to 10 nM) in aqueous solution was obtained. This LOD result found to be much lower than the maximum level of LOD (0.46 μM) of silver in drinking water, reported by the United States Environmental Protection Agency (EPA) (Y. Yang et al., 2015).

2.2. Label-free MoS_2 based biosensor

As mentioned before, each method has its own limitations in term of the applications. As representative materials in 2D TMDs, monolayer MoS_2 has attracted much attention as the sensing channel material in any label-free methods, particularly with electronic sensors such as MoS_2-FET (Gan et al., 2017). It has a unique 2D structure as well as excellent electronic properties (Mao et al., 2017) and provides a good potential impact in developing biosensing applications such as drug delivery, cancer therapy and bio-imaging.

Biosensor based on FET-devices utilizing 2D MoS_2 as a transducing platform can be attributed to the variation of charge or mass on top of the thin film surface, to adjust the area beneath the resistive channel, hence transconductance varies (Kalantar-Zadeh and Ou, 2016). To stress the advantage of biosensors mechanism, 2D FET biosensors proved to show label-free biosensing and employed for sensing proteins, DNA and other biochemical components (Kalantar-Zadeh and Ou, 2016). Indeed, label-free FET has nothing to do with the electrochemical and fluorescent tags, hence create a simpler measurement for fast detection. In comparison to label-free detection strategies, the conventional label-based methods, such as, ELISA has drawbacks. Major disadvantages include higher operating costs and real-time monitoring is limited (Wang et al., 2014).

The TMD material such as MoS_2 can enhance the sensitivity of biosensor devices (Kumar et al., 2015; Radisavljevic et al., 2011), related to the bandgap in TMDs which contributes to high sensitivity level for biomolecular target detection compared to the zero bandgap of graphene (J. Lee et al., 2015). In the year 2014, Wang et al. (2014) was the first group who demonstrated biofunctionalization molybdenum disulfide-based field effect transistor (MoS_2-based FET) as well as the sensor application in the liquid phase They have reported the invention of multilayer MoS_2-based FET for the label-free and highly sensitive detection cancer marker. This group also has done the MoS_2 synthesization process by applying mechanical exfoliation from the bulk MoS_2. The immobilization strategy between the prostate-specific antigens (PSA), the antibody, to the surface functionalization of MoS_2, resulting in the change of transistor drain current (I_d). Excellent results were achieved where the biosensor device was close to immediate detection feedback, the high sensitivity of measurement, and the high specificity for biomolecules binding phenomenon [Fig. 4 (1)]. Fig. 4 (1) a), b), and c) show the structures of MoS_2-based FET and optical image of multilayer MoS_2 structure with 14 μm size of channel width (Wang et al., 2014) with an average thickness of MoS_2 flakes is around 28 nm. Fig. 4 (1) d) shows the conductance against time of the device response when the PSA target was supplied to the microfluidic channel at various concentration of 3.75 nM, 37.5 pM and 375 fM. In addition, the change in Ids was affected by the concentration of PSA solution, and the concentration-dependence behaviour is summarized in Fig. 4 (1) e). They also reported the surface modification of HfO_2 on the MoS_2 surface with the silane-based covalent coupling of monoclonal antibodies, to build

the surface aldehyde groups, which further reacted with amino groups on the anti-PSA antibodies (Wang et al., 2014). HfO_2 layer is commonly used due to its bandgap of 5.7 eV and high-k gate dielectric high dielectric constant. In order to activate the biofunctionalization on the sensing surface, the prepared chip was immersed in 3-Triethoxysilypropylamine (APTES) solution ((Nam et al., 2015; Wang et al., 2014) and followed by glutaraldehyde (GA) solution in coupling buffer and washed (Wang et al., 2014).

Another report by Nam et al. (2015) made a performance comparison of HfO insulating-layer-coated and HfO insulating layer-free for TNF-a. molecules detection [Fig. 4(b)]. The MoS_2 layer (5–7 nm) is deposited to host the antibody receptor (monoclonal Anti-Human TNF-a) on the channel, connecting the source to drain as illustrated in Fig. 4 (2) a) and optical images in Fig. 4 (2) b) and c). For insulating-coated-layer, the graph is shifted along Vg-axis with the incremental concentrations (0–60 pM). This indicates that antigen molecules electrostatically affecting those free carrier concentrations through the MoS_2 channel [Fig. 4 (2) d)]. However, for insulating-layer-free, the outcome exhibits a different response, where the graph pattern is shifted along the Ids-axis with the incremental of concentrations [Fig. 4 (2) e)]. The result indicates the reduction of the mobility response when the TNF-a molecules are bounding to the HfO_2 layer sensor.

The result is further supported through simulation, which proved that 30 nm insulating-layer-coated forming uniform potential distribution and resulting relatively flat equipotential surfaces along the MoS_2 channel. In comparison, in HfO_2 layer-free FET, the disordered potential distribution is generated in the MoS_2 channel which causes the localization and scattering probabilities of active carriers, and degrades the carrier mobility (Nam et al., 2015).

MoS_2 -based label-free FET for DNA detection also demonstrated by another group (Lee et al., 2015; Nuzaihan et al., 2016). In the project, Lee et al. (2015) developed chemical synthesis method and deposited the material on the sensing channel, which has successfully contributed to a high sensitivity for the electrical detection of DNA hybridization. Instead of fabricating the gate oxide layer, direct immobilization of MoS_2 surface with the target DNA molecule has improved the surface charges coupling with the channel conductance. As a result, the sensitivity of 17 mV/dec was achieved at a low concentration of target DNA molecules (10 fM) (Lee et al., 2015). [Fig. 4 (3)]. Fig. 4 (3) a) shows a diagram of a FET structure using MoS_2 sensing-channel (Lee et al., 2015). Fig. 4 (3) b) shows Id-Vg characteristic values of drain current are proportionally decreased with increasing concentration, by adding a complementary target, immobilized with the probe DNA molecules and hybridized (concentration ranging from: 10 fM to 10 nM). Result in Fig. 4 (3) c) indicates the hybridization process between target and probe DNA molecules, effectively caused a shifting in Vth correspond to the concentration of complementary, non-complementary and single-base mismatched DNA molecules. Park et al. (2016) introduced high-performance Cu^{2+}-DNA/MoS_2 hybrid-based bio-FET structure. The copper ions (Cu^{2+}) was selected to induce a positive (+ve) polarity in the DNA (receptor). This method helps to enhance the detecting capability for doxorubicin- like molecules containing negative (-ve) polarity. The proposed device claimed to provide high sensitivity, excellent reusability and suitable for biosensing appliances. (Huang et al., 2013; Lin et al., 2016) also reported that CO_2 reduction process of modified copper electrode revealed a robust dependence on the initial thickness of the Cu_2O layer.

In another paper, related to detection of PSA, Lee et al. (2015) demonstrated an easy and simpler bottom-gated MoS_2 FETs device structure by mechanical exfoliation from bulk MoS_2 using scotch tape. The MoS_2 flakes were extracted within the range of 20–80 nm of thickness. Then, the detached flakes are deposited on highly doped p-Si substrate accompanied by SiO2 layer. For the surface functionalization, this team has conjugate additional APTES coupled with oxygen plasma-cleaned Si surface to achieve terminal amine group. This step is necessary due to low-affinity protein surface affinity on SiO_2. Fig. 5 (1) a) shows schematic of antigen/antibody PSA binding event, functionalized with MoS_2 surface for detecting label-free immunoassay with SiO_2 gate insulator (300 nm)/metal contact Ti/Au (15 nm/ 300 nm). Fig. 5 (1) b) shows the behaviour of the Ids-Vgs during the immobilization of antibody (anti-PSA at 100 μg/mL, PSA at 10 ng/mL) on the device surface under -32 V to 0 V back-gate bias. In Fig. 5 (1) c), the Id-Vds output response revealed 10-fold reduction at a fixed amount of PSA antigen which is 10 ng/mL at lower back-gate bias within a range of -32 V to 0 V of Vgs. It shows the results in transistor characteristics after the binding of PSA antigen, showing the sensing response is higher with increasing PSA concentrations. The adsorption of PSA on the anti-PSA immobilized sensor was depending on the concentration of PSA. They reported the limit of detection was obtained at 1 pg/mL via off-current electrical validation.

In recent times, MoS_2-based label-free FET biosensor detection using biomarker miRNA-155 to trigger an early signal of breast cancer has been proposed by Majd et al. (2018). Recently, these experts have applied liquid exfoliation technique to detach the nanosheets MoS_2 from the bulk MoS_2 (Majd et al., 2018). For fabrication procedures, immobilization of probe miRN155 onto the MoS_2 was implemented by physically adsorbed on the basal layer of MoS_2. In addition, it also presence low response signal at one-base mismatch sequence. The target miRNA-155 measurement was successfully analysed in both human serum and cell-line samples. Fig. 5 (2) a) demonstrates the fabricated MoS_2-based biosensor and Fig. 5 (2) b) captured SEM image of few-layer MoS_2 flakes on the surface electrodes (Majd et al., 2018). Fig. 5 (2) c) shows the measurement of Id-Vd of the device under wet condition. An electrolyte solution of 0.01 M PBS was transferred onto the active channel material surface in order to observe the device performance. Different back gate voltages were biased ranging from 0 V to 5 V, 1 V step. They have concluded that the device was greatly controlled under a wet environment. Also, it has good characteristics with the low driving voltage. The graph in Fig. 5 (2) d) depicts the transfer characteristics measurement of miRNA-155 hybridization by adding complementary miRNA-155 strands on the biosensor and functionalized with the probe miRNA- 155, Vback gate ranging from 0 V to 1 V, Vd = 0.1 V, concentration ranging from 0.1 fM to 10 nM. As a result, the drain current increased, the effective gate field increased, and the charge scattering reduces in the MoS_2 channel. They have reported the LOD value achieved was 0.03 fM. Referring to Fig. 5 (2) e), the sensitivity of miRNA-155 hybridization in the device was 10.976 1/decade. The sensitivity value found to be higher than one-base mismatch miRNA-155 hybridization which is 1.847 1/decade. This has proven with a better capability of biosensor towards the complementary sequence of miRNA-155.

Photoelectrochemical (PEC) sensing is an analytical method, conducted under simple operation and low-cost instrumentation. It has great potential in medical diagnose and pollutant monitoring (Li et al., 2019). In this regard, novel label-free PEC biosensors based i) graphite-like carbon nitride (C3N4)-MoS_2 heterojunction/CdSe quantum dots electrode/t-DNA; and ii) MoS_2-nitrogen-doped graphene hydrogels (NGH) heterostructure/ITO/CAP; have been developed by Li et al. (2019) and Liu et al. (2018) for detections of target DNA and chloramphenicol, respectively. These sensitive PEC biosensors achieved the LOD at 0.32 pM (S/N = 3), linear concentration ranging from 1 pM to 2 pM and LOD at 3.23 ng/L, linear concentration ranging from 32.3 ng/L to 96.9 microg/L, respectively.

In summary, the MoS_2 nanosheets-based FET promises a high sensitivity and good selectivity for label-free, real-time detection of biomarkers. Also, extensive application in disease marker detection contributes to the potential towards the point-of-care diagnostic platform with the usage of versatile HfO_2 silane-based biofunctionalization scheme. On the other hand, an additional chemical, such as APTES (3-aminoproplytriethoysilane) is needed on the oxide surfaces to control the binding actions and introduce an extra molecules layer, which can further rise the separation between charge biomolecule lamination and

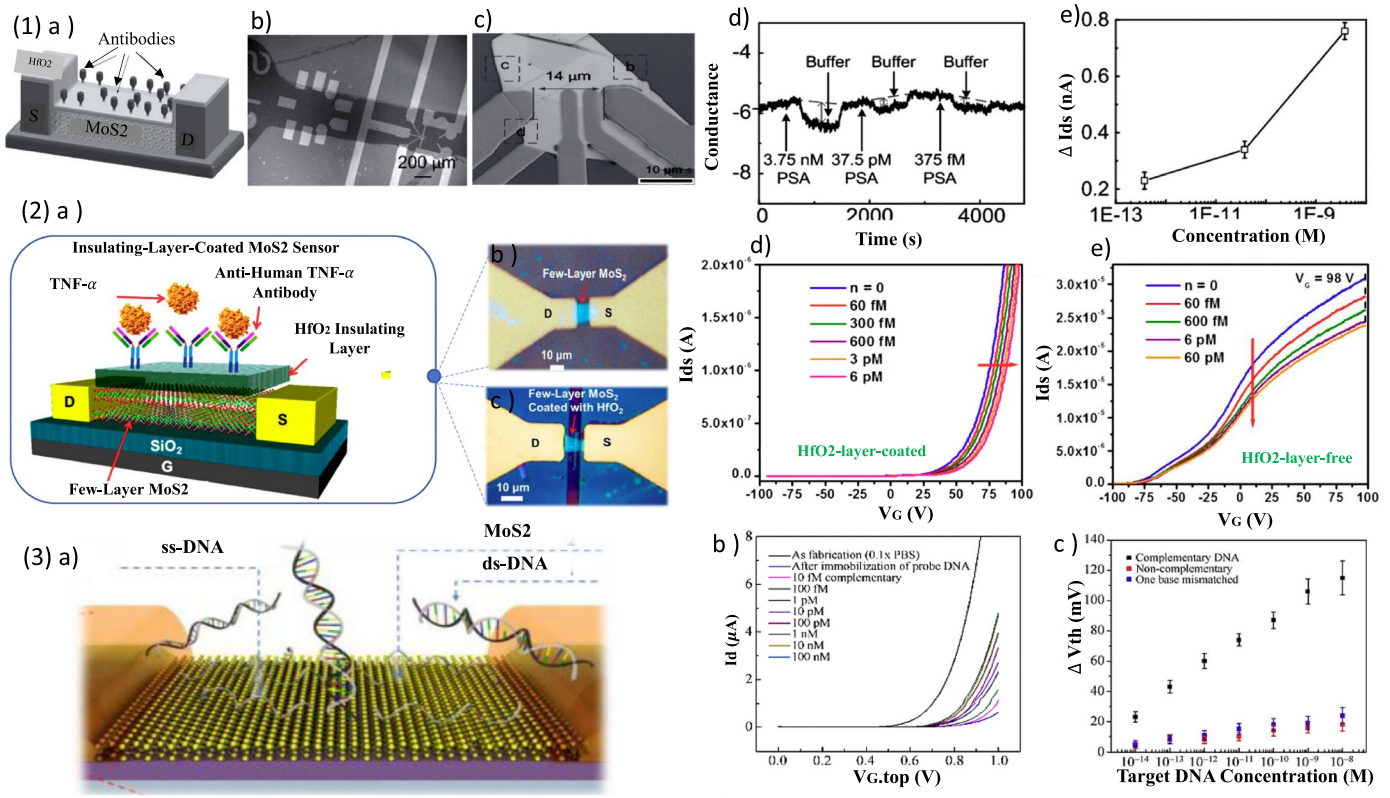

Fig. 4. (1)(a) Illustration of biofunctionalization layers on MoS_2-FET surface (b) Sensor chip image after biosensing test by using SEM (c) Optical image of the MoS_2 based FET before the deposition of HfO2 layer (d) High concentration of blocking agent Bovine Serum Albumin (1 μg/mL, i.e., 15 nM BSA) for controlling sensing experiment (e) The change of drain current absolutely depend on the PSA concentration (Wang et al., 2014). Copyright 2014 John Wiley & Sons, Inc. (2)(a), inset (b) and (c) The illustration of biosensor with HfO2 insulating-layer-free and HfO2 insulating-layer-coated (d) Ids-Vg curve for HfO2 layer-free sensor exhibit to significantly shifted along Ids-axis (e) Ids-Vg curve for HfO2 layer-coated sensor exhibit to significantly shifted along Vg-axis (Nam et al., 2015). Copyright 2015 AIP Publishing LLC (3)(a) Schematic of MoS_2-based FET, DNA hybridization (b) Illustration of MoS_2 FETs transfer characteristics, by adding complementary target, immobilized with the probe DNA molecules and hybridized (concentration ranging from: 10 fM to 10 nM) (c) Analysis of threshold voltage (Vth) correspond to the concentration of complementary, non-complementary and single-base mismatched DNA molecules. (Lee et al., 2015). Copyright 2015 Nano Research.

sensor surfaces, hence, increase the sensitivity as well as the sensor effectiveness (Lee et al., 2015). In additional, PEC biosensor also has an excellent potential to exhibit high specificity, excellent sensitivity, and low cost in biosensor DNA analysis and other relative fields (Jiang et al., 2018; Li et al., 2018).

2.3. Stability and sensitivity enhancement in MoS_2

2.3.1. Polydopamine (PDA)

Polydopamine (PDA) is one of the most versatile materials, recognized as a mussel-inspired polymer which possesses the interlayer interactions or ad-layer to act as a reducing agent and stabilizer to enhance the coating stability (Li et al., 2019; Zhang et al., 2019). This chemical/physical cross-linkage has plenty of reactive catechol groups and commonly immobilized via Micheal addition reaction (Li et al., 2019; Zhang et al., 2019). PDA provides a feasible way for covalent biofunctionalization of nanomaterials, inclusive of MoS_2, promising great potential in developing high-performance biosensors. Li et al. (2019) has demonstrated the MoS_2 @PDA-PEG-Peptide (MPPP) biosensor based on fluorescence resonance energy transfer (FRET) for caspase-3 detection. They have reported that the utilization of PDA as a nano-bio interface providing high sensitivity and selectivity of detection. They have revealed the performance of LOD value was 0.33 ng/mL. Thiol-containing peptides (FAM-labelled substrate peptide with caspase-3 specific cleavage sites and cell-penetrating peptide (TAT)) has improves the performance of peptides conjugation by 3.08 times, elevates the colloidal stability of MoS_2 @PDA. In contrast, Zhang et al. (2019) proposed polyethersulfone (PES) coating in conjugation to PDA, to support the MoS_2-PDA-TiO2 composite particles. PES is a promising engineering material providing good chemical inertness and chemical stability which are dominantly used in the super-hydrophobicity field.

2.3.2. Poly(diallyldimethylammonium chloride) (PDDA)

Poly(diallyldimethylammonium chloride (PDDA) is strong polyelectrolyte which is act as water-soluble quaternary ammonium and strong positive charged electrolyte (Feng et al., 2014; Zhang et al., 2012). Feng et al. (2014) reported that PDDA has the potential to bind with negatively charge mesoporous carbon (MC) to restrain aggregation (Zheng et al., 2015) of MC though repulsion of electrostatic. Also, PDDA helps to promote more hydrophilicity of graphene resulting in high conductivity and surface area of the graphene sheet surface (Zhang et al., 2012). Therefore, Pei et al. (2019) has included the PDDA material into their study for early detection of hepatocellular carcinoma (HCC). Biomarker AFP has been used for diagnosing HCC. In this study, they have developed a label-free immunosensor based (Pt NDs/PDDA/MoS_2 @PPy NTs) to detect alpha-fetoprotein (AFP) sensitively. This methodology has included nanocomposite of platinum nanodendreites (Pt NDs) and MoS_2 nanosheet to improve the catalytic activity. Also, polypyrrole nanotubes (PPy NTs) and poly(diallyldimethylammonium chloride) (PDDA) has been conjugated to increase electron transfer and enhanced stability. Low detection limit of 17 fg/mL has been detected with a wide linear concentration of AFP ranging from 50 fg/mL to 50 ng/mL. It shows good reproducibility, selectivity and stability. This structure showed effective immobilization of antibodies, which amplified the signal of current. The good analysis results of human serum samples implied that the immunosensor had bright potential application in clinical monitoring

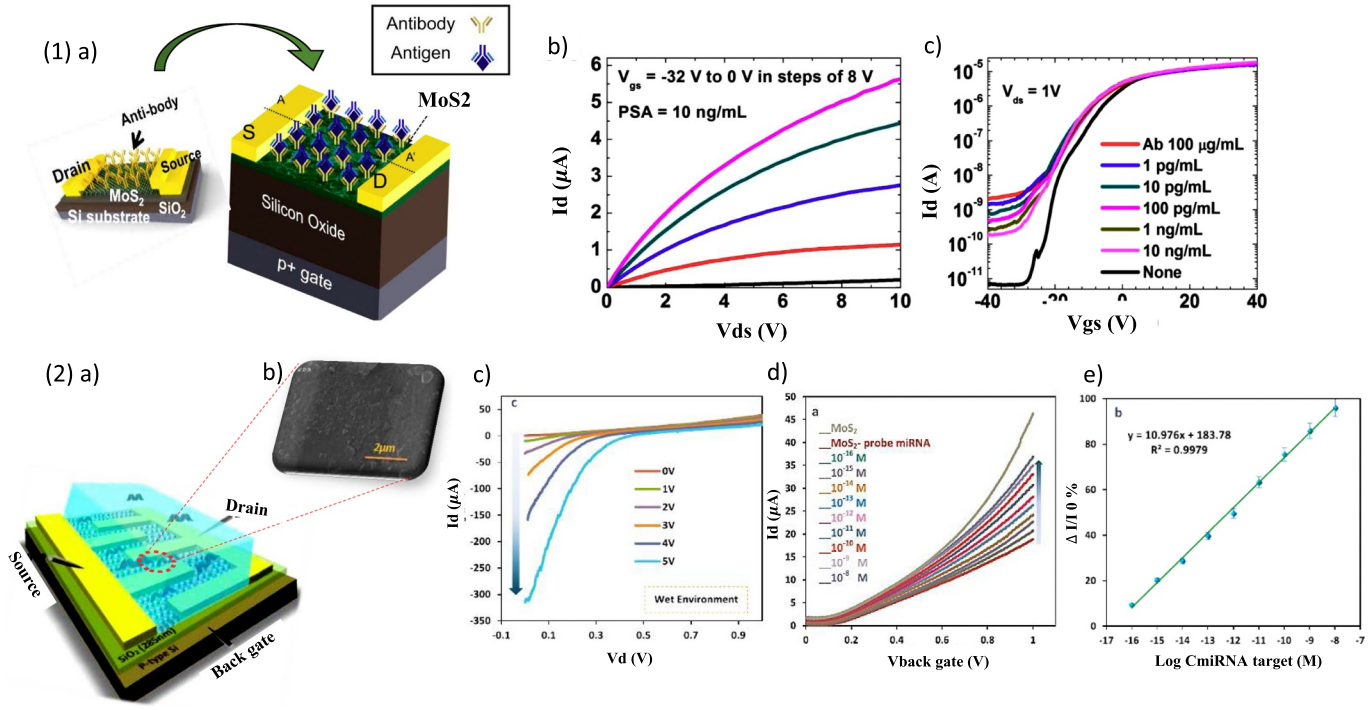

Fig. 5. (1)(a) Schematic of antigen/antibody PSA binding event, functionalized with MoS_2 surface, detecting label-free immunoassay, SiO2 gate insulator (300 nm)/ metal contact Ti/Au (15 nm/ 300 nm) (b) MoS_2 transistor transfer characteristics with the functionalization of 100 μg/mL anti-PSA under control with various PSA concentrations under -32V to 0 V back-gate bias. It gives rise to the off-current value (c) within range of -32V to 0V of Vgs, the Id-Vds output response revealed 10-fold reduction at a fixed amount of PSA antigen which is 10 ng/mL. (Lee et al., 2015). Copyright 2015 Natural Publishing Group (2)(a) and (b) An illustration for MoS_2-based FET device and MoS_2 image onto electrodes surface by capturing using SEM. (c) Different biases of Vback gate supplied (0–5 V) to the device for Id-Vd transfer curves, under wet environment measurement of PBS (pH 7.4;0.01 M) (d) Responses Id-Vback gate for incubation of probe-MoS_2 and target of miRNA-155 strands, with different concentrations of target ranging from 10^{-16} M to 10^{-8} M measured in PBS, Vd = 0.1V, and its corresponding calibration curve (e) (Majd et al., 2018). Copyright 2018 Elsevier B.V.

biomarkers. (Zhang et al., 2012) has demonstrated PPDA functionalized graphene (GR) immobilized with metallic cobalt pyrite (CoS_2) nanoparticle and MoS_2 nanosheets (CoS_2-MoS_2-PDDA-GR) via GCE and achieved detection limit as low as 6.7 × 10 − 10 mol/L(S/N = 3) for eriocitrin detection. Without CoS_2 nanoparticle conjugation (MoS_2-PDDA-GR), this group (Feng et al., 2014) had revealed the LOD value at 0.036 μmol/L (S/N = 3) with the concentration ranging from 0.1 μmol/L to 440 μmol/L for eugenol detection.

2.3.3. Polyaniline (PANI)

Polyaniline (PANI) is of the prominent conducting polymer, which is build up from two aniline molecules to form structural repeating units composition (Dutta et al., 2018; Swaminathan and Balasubramanian, 2018) utilizes within MoS_2 to offer better chemical stability, to provide great electrochemical activity, biocompatibility, and act as a protection to ambient environment (Dutta et al., 2018; T. Yang et al., 2015). In this paper, Soni et al. (2018) demonstrated an electrochemical genosensor based on PANI nanospindles (PANI-NS)-MoS_2 nanocomposites for chronic myelogenous leukemia (CML). EIS technique was selected in this project to analyse the binding interactions between pDNA/(PANI-NS)-MoS_2/ITO bioelectrode. As a result, this biosensor exhibits excellent sensitivity with LOD of 3 × 10^{-18} M and wide detection range of target DNA which is from 10^{-6} M to 10^{-17} M. This viable device is applicable for clinical diagnostics and analysations. Due to its stable structure during charge and discharge activity of PANI, Dutta et al. (2018) have fabricated an ultrasensitive electrochemical biosensor for single-stranded DNA immobilization and detection of targeted DNA hybridization by using MoS_2 nanosheets-PANI nanocomposites. Performance of DNA binding interactions using platinum electrode coated-MoS_2-PANI are shown and the device works well at concentrations as low as 10^{-15} M of target DNA. Moreover, this easy and cost-effective device also has the capability to identify any DNA mismatch in near future. Hun et al. (2018) and Yang et al. (2015) have successfully demonstrated utilized the composition of MoS_2 and polyaniline for glutathione (gold electrode) and chloramphenicol (carbon paste electrode based) detection, respectively. The LOD obtained from these two sensors were 3.1 × 10^{-11} mol/L and 6.9 × 10^{-8} mol/L, respectively.

2.3.4. MoS2 mediated signal enhancement in aptasensor

Recently, aptamers have been identified as potential robust alternatives and promising molecular recognition and detection over antibodies and showed their superiority, such as good thermal stability, low molecular weight, high selectivity, as well as low-cost and high affinity (Kenry et al., 2016; Xiang et al., 2015). These advantages are surely crucial for the diagnostic application and precise clinical sensing (Xiang et al., 2015). Fortunately, this viable device has been progressively identified to diagnose the early stage of malaria infectious illness (Kenry et al., 2016). Therefore, Kenry et al. (2016) developed the detection of Plasma lactate dehydrogenase (pLDH) protein via single-layer MoS_2-based FRET has been proposed by. It offers a sensitive and rapid detection of the target protein. As a result, the detection of the pLDH target has been reported to be successfully completed within 10 min ((Kenry et al., 2016). Geldert and Lim. et al (2017) reported a disposable and facile MoS2-FRET-based paper aptasensor for detection of the malarial biomarker, a pLDH aptamer. In this research, different types of paper have been evaluated, inclusive of scientific-grade products and commercially-available. They observed that printed paper was able to generate specific and measurable fluorescence recovery, while there was no fluorescence recovery produced on sensors shaped from other kinds of paper, such as a lens, chromatography, and filter papers. Su et al. (2016) applied different strategy, where two types of

aptamer probes labelled with Mb and Fc (double-strand and hairpin) structures have been used for adenosine triphosphate (ATP) and thrombin detection. This dual-target detection was based on AuNPs-MoS_2 nanocomposites structure. These two aptamer probes were simultaneously immobilized on the AuNPs-MoS_2 film modified electrode via an Au-S bond. This advance aptasensor capable to simultaneously verify high selectivity of thrombin and ATP as low as 0.0012 nM and 0.74 nM, respectively. Hence, the proposed aptasensor is considerable for sensitive, simple, and cost-effective detection of numerous aptamers of specific binding targets.

2.3.5. MoS_2 mediated high performance by gold-conjugation

The hot plasmonic electron of Au nanoparticles injected on the MoS_2 monolayers changes the photoluminescence characteristics and absorption behaviour of the material, resulting in n-doping Li et al. (2015) This phenomenon allows active light control of molybdenum disulfide exciton band energy. Also, the use of gold material contributes to the high affinity of biosensor devices, (Kukkar et al., 2016). These inspirational features pave the way for advance biosensors conjugating with AuNPs. The AuNPs@MoS_2 nanocomposite-modified electrode has been presented by (Su et al., 2013) for detection of for dopamine (DA), with sensitive detection as low as 80 nM (S/N = 3). This excellent sensitivity can effectively separate the ascorbic acid (AA) and dopamine (DA) oxidation potentiality. Besides, Kukkar et al. (2016) has demonstrated gold screen-printed electrode with the modification of MoS_2 flakes to detect BSA (the most abundant protein produced from the liver), and serve as iron-binding protein agent. In this experiment, they used polyclonal antibody extracted from rabbit. Polyclonal antibodies act as a complex mixture of antibodies for multiple specificities (Bamoulid et al., 2017; Delahaut, 2017). As a result, the current was increased with the increasing of BSA concentration and covering a wide range of target concentration. Hence, they successfully achieved 0.006 ng/mL of LOD at 0.01 ng/mL to 10 ng/mL of concentration range.

Luo and Davis et al. (2013) reported that screen-printed electrode (SPE) with the modification of gold nanoparticles (AuNP) have been utilized for capacitive sensor fabrication and receptor immobilization. The deposition of citrate-capped gold nanoparticles on SPE may increase the capacitance reading after the binding of cardiac troponin (cTn1) to its immobilized antibody (Luo and Davis, 2013). As a result, the limit of detection (LOD) was obtained to be 0.2 ng/mL for cTn1 target detection (Luo and Davis, 2013).

By using a screen-printed electrode, Fig. 6a) displays the morphological characterization by using FE-SEM (Kukkar et al., 2016). The formation of MoS_2 small nanosheets can be seen through the images given. Thus, this selected process resulted in a fair degree of bulk MoS_2 exfoliation into nanoflakes when the film thickness evaluated to be around 15–20 nm. Fig. 6b) illustrates the application of MoS-based electrochemical, modification of gold-screen-printed electrode with MoS_2 nanosheets. Fig. 6c) exhibits the linear response of CV corresponds to antibody BSA/MoS_2-SPE in varying concentrations of BSA ranging from 0.01 ng/mL to 10 ng/mL, in the presence of $Fe^{3+/}$ Fe^{2+} redox probe. This result describes the increment of peak current in both redox peaks with increasing BSA antigen concentrations, thus stimulated redox reaction. The redox reaction led to the improvement of the overall migration of target BSA to the SPEs surface. Linear range from 0.01 ng/mL to 10 ng/mL of antigen concentrations has been observed through Fig. 6d) and e). In this experimental study, the limit of detection found to be 6 pg/mL@0.15ng (absolute mass). Therefore, worth to mention that highly sensitive of BSA detection was achieved for BSA/anti-BSA conjugated with MoS_2-SPE modification.

3. Future perspective

Nowadays, numberless of research works were reported on the advancement in biosensor devices aided by MoS_2 material. This 2D material has attracted a tremendous interest among researchers due to its

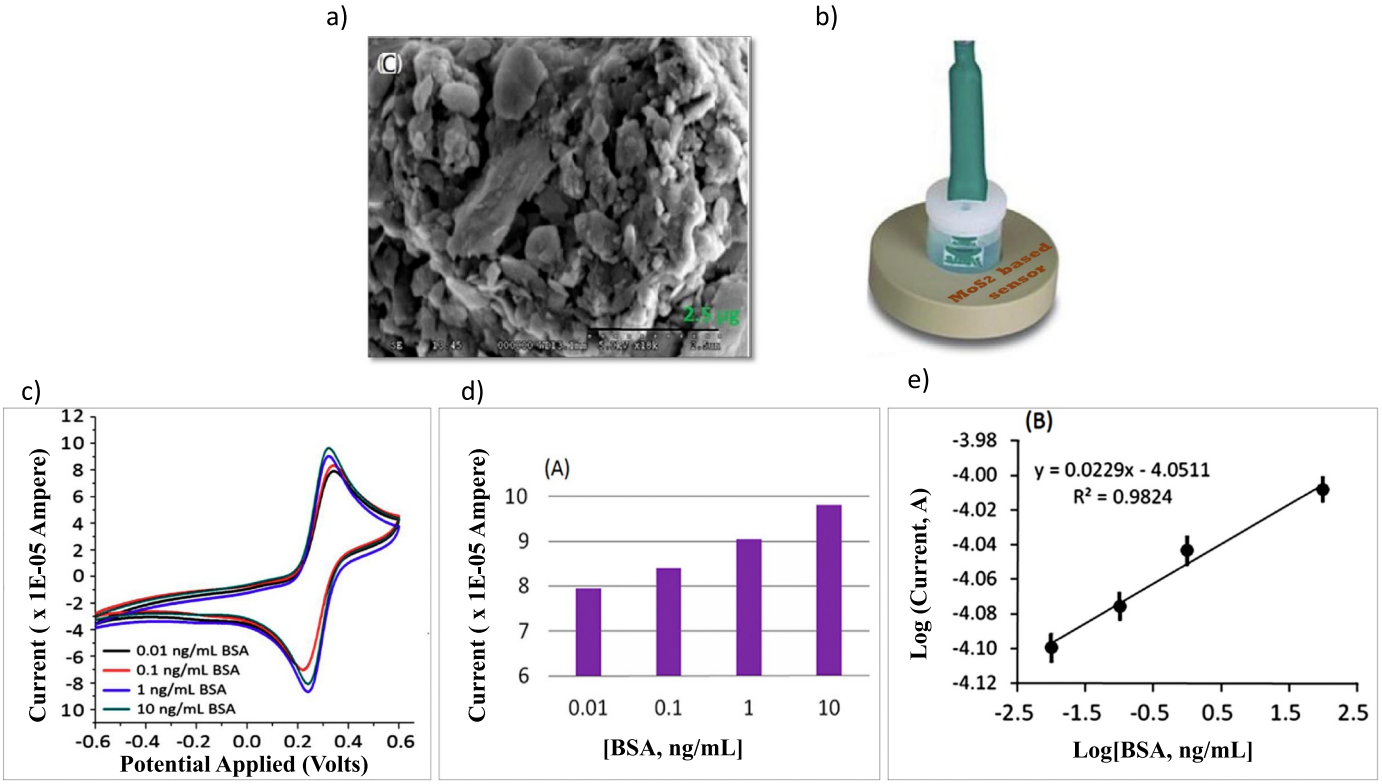

Fig. 6. (a) FE-SEM measurement for MoS_2 nanoflakes characterization (b) MoS_2-based electrochemical, screen-printed gold electrodes (SPEs)(c) The cyclic voltammograms response for anti-BSA/MoS_2 SPEs with varying BSA concentrations ranging from 0.01 ng/mL to 10 ng/mL. (d) The response to sensor as a function of varying concentrations of BSA, and its corresponding calibration curve (e). (Kukkar et al., 2016). Copyright 2016 Elsevier B.V.

fascinating chemical and physical characteristics. Despite its excellent achievement in both material properties and structure engineering, producing a rate of ultrathin two-dimensional nanomaterials are still far from the industry requirement for the commercialization (Sajid et al., 2017). Extracting the controlled layers, edge, thickness, shapes, dimensions, and dispersion volume in 2D nanosheets are still remained a challenge. In particular, synthesizing and getting good edge sites of MoS_2 are difficult and challengeable. Many studies have reported that exposing high-density active edge sites is crucial to allow the conduction of electron on the sensing surface. Therefore, one of the possible solutions was reported by Zeng et al. (2019) to perform in situ synthesis of abundant edge sites of MoS_2 via constructing sustainable solar-driven microbial fuel cell. As a result, high current density and increase interlayer spacing resulting in a high density of MoS_2 active edge sites, thus, resulting in great catalytic activity towards the hydrogen evolution reaction HER (Zeng et al., 2019; Zhou et al., 2016). In additional, extracting controlled single or few layers MoS_2 to nanometer sizes are still at the limit and demanding. Kaur et al. (2019) has confirmed an exfoliation process of MoS_2 from bulk to few layers (5–6 layers) via reduction-sulphurization method in a specially designed autoclave (700 °C, 10 h). This proposed synthesized method exhibiting a band gap of 2.29 eV and serve as a highly stable catalyst for HER through water splitting in both acidic and alkaline medium. Another important performance feature needs to be considered is the stable dispersion of exfoliated MoS_2 nanoflakes. Standard liquid phase technique by using common organic aqueous (such as NMP and DMF) are vigorously being applied in synthesization fields. However, synthesizing high-quality and stable dispersion of MoS_2 are still in progression state. In this regard, Kathiravan et al. (2019) reported sericin-assisted liquid phase exfoliation induces robust interaction between the material and the solvent, presenting high dispersion stability of MoS_2. Also, this sericin-coated MoS_2 strategy exhibits great H_2 sensing properties with long term stability, good sensitivity and repeatability. Besides, Wang et al. (2019) reported that stable dispersion of functional MoS_2 nanosheets can be maintained over long periods of time via a combination of liquid phase exfoliation method and thiol-containing molecules. This suggested mixture to enhance the performance of the water-based lubricant.

From the biosensing performance point of view, ultrathin MoS_2 nanosheets on sensing surface are a lack in stability and poor reusability because the structural change or decomposition may occur during the chemical reaction (Barua, 2017; Hamdi et al., 2017; Sha et al., 2019). In order to rectify this issue, hybridize the MoS_2 nanosheets with other polymer materials to form nanocomposites/hetero-nanostructures is such a great move to overcome this drawback. Therefore, stabilizer agents, such as, polymer materials play an important role to enhance sensitivity and electron transfer as well as to improve the catalytic activity on the surface. Versatile biofunctionalization strategies of nanocomposites polymers into MoS_2-based biosensors promising good stability, sensitivity, and selectivity of various biomarkers detection PDA coating accommodates a feasible move for covalent biofunctionalization of MoS_2 nanomaterials. PDA also consists largely of reactive catechol groups, promising excellent potential in developing high-performance biosensors (Li et al., 2019).

Besides, nanostructure PANI contributes to good structural stability and great adsorption ability. Nonetheless, insolubility and poor mechanical strength of PANI give a limitation to the viable applications. In this case, Soni et al. (2018) reported hybrid nanostructure of PANI with MoS_2 can possibly solve this drawback. This synergistic effect between the nanocomposite conjugation performing good electrocatalytic ability for biosensors. Recently, CdS QDs functionalized oxide-polyaniline composite has been developed for detection of the K562 cell line. This study performing high intensity of detection signal and tumour cells ratio. Similarly, another conducting polymers materials such as PDA and PDDA also have been widely used for MoS_2 biofunctionalization sensors (Pei et al., 2019; Zhang et al., 2019). On the other hand, small functional biomolecules such as guanosine monophosphate (GMP), adenosine monophosphate (AMP), and flavin mononucleotide (FMN have been utilized to stabilized the MoS_2 nanoflakes (Paredes and Vila, 2019).

4. Conclusion

Mos_2 has been widely used as a transducer material due to its tremendous properties such as, large surface areas, ultrathin plane structure, large surface-to-volume ratio, appreciable band gap, high carrier mobility, low noise level, low contact resistance, and good edge contact between the metal. These advantages promote excellent conductivity as well as enhanced the sensitivity of immunosensors. On the other hand, MoS_2 nanocomposite materials for enzyme immobilization (conducting polymers such as PDA, PDDA, PANI) allowing better biofunctionalization stability of MoS_2-based biosensors, hence, paves the way for the enhancement in modern next-generation electronic and optoelectronic. Nevertheless, there are still plenty of biosensing mechanisms, concepts and applications are not being discovered yet potentially studied. Albeit a large number of MoS_2-based biosensors invention was reported in the recent literature, it is foreseeable that in the future there will be a focus and interest of researchers towards the performance of electrochemical energy storage, signal enhancement, and electrocatalytic efficiency and edge site activity.

CRediT authorship contribution statement

N. Dalila R: Conceptualization, Data curation, Formal analysis, Writing - original draft, Writing - review & editing. **M.K. Md Arshad:** Conceptualization, Data curation, Funding acquisition, Project administration, Supervision, Validation, Writing - review & editing. **Subash C.B. Gopinath:** Data curation, Supervision, Validation, Writing - review & editing. **W.M.W. Norhaimi:** Supervision, Validation. **M.F.M. Fathil:** Supervision, Validation.

Acknowledgements

The author would like to acknowledge the support from the Fundamental Research Grant Scheme (FRGS) under a Grant no. of FRGS/1/2017/STG05/UNIMAP/03/3 from the Ministry of Education Malaysia.

Declaration of interest statement

None.

References

Adzhri, R., Md Arshad, M.K., Gopinath, S.C.B., Ruslinda, A.R., Fathil, M.F.M., Ayub, R.M., Nor, M.N.M., Voon, C.H., 2016. High-performance integrated field-effect transistor-based sensors. Anal. Chim. Acta 917, 1–18. https://doi.org/10.1016/j.aca.2016.02.042.

Ambrosi, A., Chia, X., Sofer, Z., Pumera, M., 2015. Enhancement of electrochemical and catalytic properties of MoS_2 through ball-milling. Electrochem. Commun. 54, 36–40. https://doi.org/10.1016/j.elecom.2015.02.017.

Amini, M., Ramazani, S.A., A., Faghihi, M., Fattahpour, S., 2017. Preparation of nanostructured and nanosheets of MoS_2 oxide using oxidation method. Ultrason. Sonochem. 39, 188–196. https://doi.org/10.1016/j.ultsonch.2017.04.024.

Bamoulid, J., Crepin, T., Gaiffe, E., Laheurte, C., Moulin, B., Frimat, L., Rieu, P., Mousson, C., Durrbach, A., Heng, A.E., Rebibou, J.M., Saas, P., Courivaud, C., Ducloux, D., 2017. Immune reconstitution with two different rabbit polyclonal anti-thymocytes globulins. Transpl. Immunol. 45, 48–52. https://doi.org/10.1016/j.trim.2017.09.002.

Barua, 2017. Nanostructured based advanced biosensors : A review. ⟨http://dx.doi.org/10.1021/acsanm.7b00157⟩.

Bhimanapati, G.R., Lin, Z., Meunier, V., Jung, Y., Cha, J., Das, S., Xiao, D., Son, Y., Strano, M.S., Cooper, V.R., Liang, L., Louie, S.G., Ringe, E., Zhou, W., Kim, S.S., Naik, R.R., Sumpter, B.G., Terrones, H., Xia, F., Wang, Y., Zhu, J., Akinwande, D., Alem, N., Schuller, J.A., Schaak, R.E., Terrones, M., Robinson, J.A., 2015. Recent advances in two-dimensional materials beyond graphene. ACS Nano 9, 11509–11539. https://doi.org/10.1021/acsnano.5b05556.

Bonaccorso, F., Lombardo, A., Hasan, T., Sun, Z., Colombo, L., Ferrari, A.C., 2012. Production and processing of graphene and 2D crystals graphene is at the center of an ever growing research effort due to its unique to these crystals, accelerating their journey towards applications. Mater. Today 15, 564–589. https://doi.org/10.1016/S1369-7021(13)70014-2.

Chang, C., Li, H., Shi, Y., Zhang, H., Lai, C., Li, L., 2012. Growth of large-area and highly crystalline MoS_2 thin layers on insulating substrates. 〈http://dx.doi.org/10.1021/nl2043612〉.

Chen, X., Park, Y.J., Kang, M., Kang, S., Koo, J., Shinde, S.M., Shin, J., Jeon, S., Park, G., Yan, Y., Macewan, M.R., Ray, W.Z., Lee, K., Rogers, J.A., Ahn, J., 2018. CVD-grown monolayer MoS_2 in bioabsorbable electronics and biosensors. Nat. Commun. 1–12. https://doi.org/10.1038/s41467-018-03956-9.

Chhowalla, M., Jena, D., Zhang, H., 2016. Two-dimensional semiconductors for transistors. Nat. Rev. Mater. 1, 1–15. https://doi.org/10.1038/natrevmats.2016.52.

Choi, W., Choudhary, N., Han, G.H., Park, J., Akinwande, D., Lee, Y.H., 2017. Recent development of two-dimensional transition metal dichalcogenides and their applications. Mater. Today 20, 116–130. https://doi.org/10.1016/j.mattod.2016.10.002.

Coleman, J.N., Lotya, M., O'Neill, A., Bergin, S.D., King, P.J., Khan, U., Young, K., Gaucher, A., De, S., Smith, R.J., Shvets, I.V., Arora, S.K., Stanton, G., Kim, H.Y., Lee, K., Kim, G.T., Duesberg, G.S., Hallam, T., Boland, J.J., Wang, J.J., Donegan, J.F., Grunlan, J.C., Moriarty, G., Shmeliov, A., Nicholls, R.J., Perkins, J.M., Grieveson, E.M., Theuwissen, K., McComb, D.W., Nellist, P.D., Nicolosi, V., 2011. Two-dimensional nanosheets produced by liquid exfoliation of layered materials. Science (80-.) 331, 568–571. https://doi.org/10.1126/science.1194975.

Delahaut, P., 2017. Immunisation – choice of host, adjuvants and boosting schedules with emphasis on polyclonal antibody production. Methods 116, 4–11. https://doi.org/10.1016/j.ymeth.2017.01.002.

Dickinson, R.G., Pauling, L., 1923. The crystal structure of molybdenite. J. Am. Chem. Soc. 45, 1466–1471. https://doi.org/10.1021/ja01659a020.

Dutta, S., Dutta, A., Biswas, S., Park, E.Y., 2018. Development of an effective electrochemical platform for highly sensitive DNA detection using MoS_2-polyaniline nanocomposites. Biochem. Eng. J. 140, 130–139. https://doi.org/10.1016/j.bej.2018.09.016.

Fathil, M.F.M., Md Arshad, M.K., Ruslinda, A.R., Nuzaihan, M., Gopinath, S.C.B., Adzhri, R., Hashim, U., 2016. Progression in sensing cardiac troponin biomarker charge transductions on semiconducting nanomaterials. Anal. Chim. Acta 935, 30–43. https://doi.org/10.1016/j.aca.2016.06.012.

Feng, Q., Duan, K., Ye, X., Lu, D., Du, Y., Wang, C., 2014. A novel way for detection of eugenol via poly (diallyldimethylammonium chloride) functionalized graphene-MoS_2 nano-flower fabricated electrochemical sensor. Sens. Actuators B Chem. 192, 1–8. https://doi.org/10.1016/j.snb.2013.10.087.

Ferrari, A.C., Bonaccorso, F., Falko, V., Novoselov, K.S., Roche, S., Bøggild, P., Borini, S., Koppens, F., Palermo, V., Pugno, N., Garrido, J. a., Sordan, R., Bianco, A., Ballerini, L., Prato, M., Lidorikis, E., Kivioja, J., Marinelli, C., Ryhänen, T., Morpurgo, A., Coleman, J.N., Nicolosi, V., Colombo, L., Fert, A., Garcia-Hernandez, M., Bachtold, A., Schneider, G.F., Guinea, F., Dekker, C., Barbone, M., Galiotis, C., Grigorenko, A., Konstantatos, G., Kis, A., Katsnelson, M., Beenakker, C.W.J., Vandersypen, L., Loiseau, A., Morandi, V., Neumaier, D., Treossi, E., Pellegrini, V., Polini, M., Tredicucci, A., Williams, G.M., Hong, B.H., Ahn, J.H., Kim, J.M., Zirath, H., van Wees, B.J., van der Zant, H., Occhipinti, L., Di Matteo, A., Kinloch, I. a., Seyller, T., Quesnel, E., Feng, X., Teo, K., Rupesinghe, N., Hakonen, P., Neil, S.R.T., Tannock, Q., Löfwander, T., Kinaret, J., 2014. Science and technology roadmap for graphene, related two-dimensional crystals, and hybrid systems. Nanoscale 7. pp. 4598–4810. https://doi.org/10.1039/C4NR01600A.

Frindt, R.F., Yoffe, A.D., 1963. Physical properties of layer structures: optical properties and photoconductivity of thin crystals of molybdenum disulfide. Proc. R. Soc. A Math. Phys. Eng. Sci. 273, 69–83. https://doi.org/10.1098/rspa.1963.0075.

Gan, X., Zhao, H., Quan, X., 2017. Two-dimensional MoS_2: a promising building block for biosensors. Biosens. Bioelectron. 89, 56–71. https://doi.org/10.1016/j.bios.2016.03.042.

Gan, X., Zhao, H., Wong, K.Y., Lei, D.Y., Zhang, Y., Quan, X., 2018. Covalent functionalization of MoS_2 nanosheets synthesized by liquid phase exfoliation to construct electrochemical sensors for Cd (II) detection. Talanta 182, 38–48. https://doi.org/10.1016/j.talanta.2018.01.059.

Geldert, A., Lim, C.T., 2017. Paper-based MoS_2 nanosheet- mediated FRET aptasensor for rapid malaria diagnosis. Sci. Rep. 1–8. https://doi.org/10.1038/s41598-017-17616-3.

Ghasemi, F., Mohajerzadeh, S., 2016. Sequential solvent exchange method for controlled exfoliation of MoS_2 suitable for phototransistor fabrication. ACS Appl. Mater. Interfaces 8, 31179–31191. https://doi.org/10.1021/acsami.6b07211.

Guine, A.D.E.L., 1897. United states patent office.

Gupta, A., Sakthivel, T., Seal, S., 2015. Recent development in 2D materials beyond graphene. Prog. Mater. Sci. 73, 44–126. https://doi.org/10.1016/j.pmatsci.2015.02.002.

Ha, H.D., Han, D.J., Choi, J.S., Park, M., Seo, T.S., 2014. Dual role of blue luminescent MoS_2 quantum dots in fluorescence resonance energy transfer phenomenon. Small 10, 3858–3862. https://doi.org/10.1002/smll.201400988.

Hamdi, A., Hosu, I.S., Addad, A., Hartkoorn, R., Drobecq, H., Melnyk, O., Ezzaouia, H., Boukherroub, R., Coffinier, Y., 2017. MoS_2/TiO_2/SiNW surface as an effective substrate for LDI-MS detection of glucose and glutathione in real samples. Talanta 171, 101–107. https://doi.org/10.1016/j.talanta.2017.04.061.

Han, J., Xia, H., Wu, Y., Kong, S.N., Deivasigamani, A., Xu, R., Hui, K.M., Kang, Y., 2016. Single-layer MoS_2 nanosheet grafted upconversion nanoparticles for near-infrared fluorescence imaging-guided deep tissue cancer phototherapy. Nanoscale 8, 7861–7865. https://doi.org/10.1039/c6nr00150e.

Hernandez, Y., Nicolosi, V., Lotya, M., Blighe, F.M., Sun, Z., De, S., McGovern, I.T., Holland, B., Byrne, M., Gun'ko, Y.K., Boland, J.J., Niraj, P., Duesberg, G., Krishnamurthy, S., Goodhue, R., Hutchison, J., Scardaci, V., Ferrari, A.C., Coleman, J.N., 2008. High-yield production of graphene by liquid-phase exfoliation of graphite. Nat. Nanotechnol. 3, 563–568. https://doi.org/10.1038/nnano.2008.215.

Huang, J., Dong, Z., Li, Y., Li, J., Tang, W., 2013. MoS_2 nanosheet functionalized with Cu nanoparticles and its application for glucose detection. Mater. Res. Bull. 48, 4544–4547. https://doi.org/10.1016/j.materresbull.2013.07.060.

Huang, Y., Sutter, E., Shi, N.N., Zheng, J., Yang, T., Englund, D., Gao, H., Sutter, P., 2015. Reliable exfoliation of large-area high-quality flakes of graphene and other two-dimensional materials. ACS Nano 10612–10620. https://doi.org/10.1021/acsnano.5b04258.

Hun, X., Li, Y., Wang, S., Li, Y., Zhao, J., Zhang, H., Luo, X., 2018. Photoelectrochemical platform for cancer cell glutathione detection based on polyaniline and nanoMoS_2 composites modified gold electrode. Biosens. Bioelectron. 112, 93–99. https://doi.org/10.1016/j.bios.2018.04.031.

Ibau, C., Md Arshad, M.K., Subash, C.B., G., 2017. Current advances and future visions on bioelectronic immunosensing for prostate-specific antigen. Biosens. Bioelectron. 98, 267–284. https://doi.org/10.1016/j.bios.2017.06.049.

IUPAC, 2014. Compendium of Chemical Terminology 2nd ed. (the "Gold Book"). Blackwell Sci. Publ., Oxford, pp. 1670. https://doi.org/10.1351/goldbook.I03352.

Jiang, D., Du, X., Qian, L., Hao, N., 2018. MoS_2/nitrogen doped graphene hydrogels p-n heterojunction: efficient charge transfer property for highly sensitive and selective photoelectrochemical analysis of chloramphenicol. 10.1016/j.bios.2018.11.018.

Joensen, P., Frindt, R.F., Morrison, S.R., 1986. Single-layer MoS_2. Mater. Res. Bull. 21, 457–461. https://doi.org/10.1016/0025-5408(86)90011-5.

Kalantar-zadeh, K., Ou, J.Z., 2016. Biosensors based on two-dimensional MoS_2. ACS Sens. 1, 5–16. https://doi.org/10.1021/acssensors.5b00142.

Kalantar-Zadeh, K., Ou, J.Z., 2016. Biosensors based on two-dimensional MoS_2. ACS Sens. 1, 5–16. https://doi.org/10.1021/acssensors.5b00142.

Kappera, R., Voiry, D., Yalcin, S.E., Branch, B., Gupta, G., Mohite, A.D., Chhowalla, M., 2014. Phase-engineered low-resistance contacts for ultrathin MoS_2 transistors. Nat. Mater. 13, 1128–1134. https://doi.org/10.1038/nmat4080.

Kathiravan, D., Huang, B., Saravanan, A., Prasannan, A., 2019. Highly enhanced hydrogen sensing properties of sericin-induced exfoliated MoS_2 nanosheets at room temperature. Sens. Actuators B. Chem. 279, 138–147. https://doi.org/10.1016/j.snb.2018.09.104.

Kaur, N., Mir, R.A., Pandey, O.P., 2019. Electrochemical and optical studies of facile synthesized molybdenum disulphide (MoS_2) nano structures. J. Alloy. Compd. 782, 119–131. https://doi.org/10.1016/j.jallcom.2018.12.145.

Kenry, Geldert, Zhang, A., Zhang, X., Lim, C.T, H., 2016. Highly sensitive and selective aptamer-based fluorescence detection of a malarial biomarker using single-layer MoS2 nanosheets. ACS Sens. 1, 1315–1321. https://doi.org/10.1021/acssensors.6b00449.

Krishnamoorthy, K., Pazhamalai, P., Veerasubramani, G.K., Kim, S.J., 2016. Mechanically delaminated few layered MoS_2 nanosheets based high performance wire type solid-state symmetric supercapacitors. J. Power Sources 321, 112–119. https://doi.org/10.1016/j.jpowsour.2016.04.116.

Kukkar, M., Sharma, A., Kumar, P., Kim, K.H., Deep, A., 2016. Application of MoS_2 modified screen-printed electrodes for highly sensitive detection of bovine serum albumin. Anal. Chim. Acta 939, 101–107. https://doi.org/10.1016/j.aca.2016.08.010.

Kumar, N.A., Dar, M.A., Gul, R., Baek, J.B., 2015. Graphene and molybdenum disulfide hybrids: synthesis and applications. Mater. Today 18, 286–298. https://doi.org/10.1016/j.mattod.2015.01.016.

Lee, D.-W., Lee, J., Sohn, I.Y., Kim, B.-Y., Son, Y.M., Bark, H., Jung, J., Choi, M., Kim, T.H., Lee, C., Lee, N.-E., 2015. Field-effect transistor with a chemically synthesized MoS_2 sensing channel for label-free and highly sensitive electrical detection of DNA hybridization. Nano Res. 8, 2340–2350. https://doi.org/10.1007/s12274-015-0744-8.

Lee, J., Dak, P., Lee, Y., Park, H., Choi, W., Alam, M.A., Kim, S., 2015. Enhancement of electrochemical and catalytic properties of MoS_2 through ball-milling. Sci. Rep. 4, 7352. https://doi.org/10.1038/srep07352.

Lee, Y.-H., Zhang, X.-Q., Zhang, W., Chang, M.-T., Lin, C.-T., Chang, K.-D., Yu, Y.-C., Wang, J.T.-W., Chang, C.-S., Li, L.-J., Lin, T.-W., 2012. Synthesis of large-area MoS_2 atomic layers with chemical vapor deposition. Adv. Mater. 24, 2320–2325. https://doi.org/10.1002/adma.201104798.

Letchumanan, I., Md Arshad, M.K., Balakrishnan, S.R., Gopinath, S.C.B., 2019. Gold-nanorod enhances dielectric voltammetry detection of c-reactive protein: a predictive strategy for cardiac failure. Biosens. Bioelectron. 130, 40–47. https://doi.org/10.1016/j.bios.2019.01.042.

Li, P., Liu, X., Mao, C., Jin, B., Zhu, J., 2018. Photoelectrochemical DNA biosensor based on g-C3N4/MoS_2 2D/2D heterojunction electrode matrix and co-sensitization amplification with CdSe QDs for the sensitive detection of ssDNA Pan-Pan. Anal. Chim. Acta. https://doi.org/10.1016/j.aca.2018.09.063.

Li, P.P., Liu, X.P., Mao, C.J., Jin, B.K., Zhu, J.J., 2019. Photoelectrochemical DNA biosensor based on g-C3N4/MoS_2 2D/2D heterojunction electrode matrix and co-sensitization amplification with CdSe QDs for the sensitive detection of ssDNA. Anal. Chim. Acta 1048, 42–49. https://doi.org/10.1016/j.aca.2018.09.063.

Li, X., Zhu, H., 2015. Two-dimensional MoS_2: properties, preparation, and applications. J. Mater. 1, 33–44. https://doi.org/10.1016/j.jmat.2015.03.003.

Li, X., Li, Y., Qiu, Q., Wen, Q., Zhang, Q., Yang, W., 2019. Efficient biofunctionalization of MoS_2 nanosheets with peptides as intracellular fluorescent biosensor for sensitive detection of caspase-3 activity. J. Colloid Interface Sci. https://doi.org/10.1016/j.jcis.2019.02.011.

Li, Z., et al., 2015. Active light control of the MoS_2. ACS Publ. 9, 10158–10164. https://doi.org/10.1021/acsnano.5b03764.

Li, Z., Wong, S.L., 2017. Functionalization of 2D transition metal dichalcogenides for biomedical applications. Mater. Sci. Eng. C 70, 1095–1106. https://doi.org/10.1016/j.msec. (2016.03.039).

Lin, X., Ni, Y., Kokot, S., 2016. Electrochemical and bio-sensing platform based on a novel 3D Cu nano- fl owers/layered MoS_2 composite 79, pp. 685–692. 10.1016/j.bios.2015.12.072.

Liu, B., Li, C., Chen, G., Liu, B., Deng, X., Wei, Y., Xia, J., Xing, B., Ma, P., Lin, J., 2017. Synthesis and optimization of MoS2@Fe3O4-ICG/Pt(IV) nanoflowers for MR/IR/PA bioimaging and combined PTT/PDT/chemotherapy triggered by 808 nm laser. Adv. Sci. 4. https://doi.org/10.1002/advs.201600540.

Liu, N., Kim, P., Kim, J.H., Ye, J.H., Kim, S., Lee, C.J., 2014. Large-area atomically thin MoS_2 nanosheets prepared using electrochemical exfoliation. ACS Nano 8, 6902–6910. https://doi.org/10.1021/nn5016242.

Liu, P., Xiang, B., 2017. 2D heterostructures based on transition metal dichalcogenides: fabrication, properties and applications. Sci. Bull. 62, 1148–1161. https://doi.org/10.1016/j.scib.2017.08.007.

Liu, Q., Hao, N., Du, X., Jiang, D., Wang, K., 2018. MoS_2/nitrogen doped graphene hydrogels p-n heterojunction: Efficient charge transfer property for highly sensitive and selective photoelectrochemical analysis of chloramphenicol. Biosens. Bioelectron. 126, 463–469. https://doi.org/10.1016/j.bios.2018.11.018.

Liu, W., Kang, J., Cao, W., 2013a. High-performance few-layer-MoS_2 field-effect-transistor with record low contact-resistance. Iedm 2013, 499–502. https://doi.org/10.1109/IEDM.2013.6724660.

Liu, W., Kang, J., Cao, W., Sarkar, D., Khatami, Y., Jena, D., Banerjee, K., 2013b. High-performance few-layer-MoS_2 field-effect-transistor with record low-contact-resistance. 2013 (19.4.1-19.4.4). IEEE Int. Electron Devices Meet. https://doi.org/10.1109/IEDM.2013.6724660.

Luo, X., Davis, J.J., 2013. Electrical biosensors and the label free detection of protein disease biomarkers. Chem. Soc. Rev. 42, 5944. https://doi.org/10.1039/c3cs60077g.

Ma, H., Shen, Z., Ben, S., 2018. Understanding the exfoliation and dispersion of MoS_2 nanosheets in pure water. J. Colloid Interface Sci. 517, 204–212. https://doi.org/10.1016/j.jcis.2017.11.013.

Mahyavanshi, R.D., Kalita, G., Sharma, K.P., Kondo, M., Dewa, T., Kawahara, T., Tanemura, M., 2017. Synthesis of MoS_2 ribbons and their branched structures by chemical vapor deposition in sulfur enriched environment. Appl. Surf. Sci. 409, 396–402. https://doi.org/10.1016/j.apsusc.2017.03.074.

Maidin, N.N.M., Rahim, R.A., Halim, N.H.A., Abidin, A.S.Z., Ahmad, N.A., Lockman, Z., 2018. Interaction of graphene electrolyte gate field-effect transistor for detection of cortisol biomarker. AIP Conf. Proc. 2045. https://doi.org/10.1063/1.5080835.

Majd, S.M., Salimi, A., Ghasemi, F., 2018. An ultrasensitive detection of miRNA-155 in breast cancer via direct hybridization assay using two-dimensional molybdenum disulfide field-effect transistor biosensor. Biosens. Bioelectron. 105, 6–13. https://doi.org/10.1016/j.bios.2018.01.009.

Mao, S., Chang, J., Pu, H., Lu, G., He, Q., Zhang, H., Chen, J., 2017. Two-dimensional nanomaterial-based field-effect transistors for chemical and biological sensing. Chem. Soc. Rev. 46, 6872–6904. https://doi.org/10.1039/C6CS00827E.

Marx, M., Nordmann, S., Knoch, J., Franzen, C., Stampfer, C., Andrzejewski, D., Kümmell, T., Bacher, G., Heuken, M., Kalisch, H., Vescan, A., 2017. Large-area MoS_2 deposition via MOVPE. J. Cryst. Growth 464, 100–104. https://doi.org/10.1016/j.jcrysgro.2016.11.020.

Mehrotra, P., 2016. Biosensors and their applications - a review. J. Oral. Biol. Craniofacial Res. 6, 153–159. https://doi.org/10.1016/j.jobcr.2015.12.002.

Nam, H., Oh, B.R., Chen, P., Yoon, J.S., Wi, S., Chen, M., Kurabayashi, K., Liang, X., 2015. Two different device physics principles for operating MoS_2 transistor biosensors with femtomolar-level detection limits. Appl. Phys. Lett. 107, 1–6. https://doi.org/10.1063/1.4926800.

Nordin, N.K.S., Hashim, U., Ruslinda, A.R., Ayoib, A., Thivina, V., 2016. Electrical Characterization of Surface Modified IDE with Gold Nano Particles, pp.185–187.

Novoselov, K.S., Geim, A.K., Morozov, S.V., Jiang, D., Zhang, Y., Dubonos, S.V., Grigorieva, I.V., Firsov, A.A., Novoselov, K.S., 2004. Electric field effect in atomically thin carbon films. Sci. (80-.) 306, 666–669. https://doi.org/10.1038/nmat1849.

Nuzaihan, M.M.N., Hashim, U., Md Arshad, M.K., Kasjoo, S.R., Rahman, S.F.A., Ruslinda, A.R., Fathil, M.F.M., Adzhri, R., Shahimin, M.M., 2016. Electrical detection of dengue virus (DENV) DNA oligomer using silicon nanowire biosensor with novel molecular gate control. Biosens. Bioelectron. 83, 106–114. https://doi.org/10.1016/j.bios.2016.04.033.

O'Neill, A., Khan, U., Coleman, J.N., 2012. Preparation of high concentration dispersions of exfoliated MoS_2 with increased flake size. Chem. Mater. 24, 2414–2421. https://doi.org/10.1021/cm301515z.

Paredes, J.I., Vila, M., 2019. MoS_2 flakes stabilized with DNA/RNA nucleotides: In vitro cell response M. Mater. Sci. Eng. C. https://doi.org/10.1016/j.msec. (2019.02.002).

Park, H., Dugasani, S.R., Kang, D., Yoo, G., Lee, S., Heo, J., Jeon, Y.J., Park, S.H., Park, J., 2016. M-DNA/transition metal dichalcogenide hybrid structure- based bio-FET sensor with ultra-high sensitivity. Nat. Publ. Gr. 1–9. https://doi.org/10.1038/srep35733.

Pei, F., Wang, P., Ma, E., Yang, Q., Yu, H., Liu, J., Yin, H., Li, Y., Liu, Q., Dong, Y., 2019. A sensitive label-free immunosensor for alpha fetoprotein detection using platinum nanodendrites loaded on functional MoS_2 hybridized polypyrrole nanotubes as signal amplifier. J. Electroanal. Chem. 835, 197–204. https://doi.org/10.1016/j.jelechem.2019.01.037.

Pradhan, G., Sharma, A.K., 2018. Anomalous Raman and photoluminescence blue shift in mono- and a few layered pulsed laser deposited MoS_2thin films. Mater. Res. Bull. 102, 406–411. https://doi.org/10.1016/j.materresbull.2018.03.001.

Radisavljevic, B., Radenovic, A., Brivio, J., Giacometti, V., Kis, A., 2011. Single-layer MoS_2 transistors. Nat. Nanotechnol. 6, 147–150. https://doi.org/10.1038/nnano.2010.279.

Roldan, R., Chirolli, L., Prada, E., Silva-Guillen, J.A., San-Jose, P., Guinea, F., 2017. Theory of 2D crystals: graphene and beyond. Chem. Soc. Rev. 46. https://doi.org/10.1039/C7CS00210F.

Sahu, R., Radhakrishnan, D., Vishal, B., Singh, D., Sil, A., Narayana, C., Datta, R., 2017. Substrate induced tuning of compressive strain and phonon modes in large area MoS_2 and WS_2 van der waals epitaxial thin films. J. Cryst. Growth 470, 51–57. https://doi.org/10.1016/j.jcrysgro.2017.04.012.

Sajid, M., Osman, A., Siddiqui, G.U., Kim, H.B., Kim, S.W., Ko, J.B., Lim, Y.K., Choi, K.H., 2017. All-printed highly sensitive 2D MoS_2 based multi-reagent immunosensor for smartphone based point-of-care diagnosis. Sci. Rep. 7, 1–11. https://doi.org/10.1038/s41598-017-06265-1.

Sang, S., Wang, Y., Feng, Q., Wei, Y., Ji, J., Zhang, W., 2015. Progress of new label-free techniques for biosensors: a review. Crit. Rev. Biotechnol. 00, 1–17. https://doi.org/10.3109/07388551.2014.991270.

Sarkar, D., Liu, W., Xie, X., Anselmo, A.C., Mitragotri, S., Banerjee, K., 2014. MoS_2 field-effect transistor for next-generation label-free biosensors. ACS Nano 8, 3992–4003. https://doi.org/10.1021/nn5009148.

Schwierz, F., Pezoldt, J., Granzner, R., 2015. Two-dimensional materials and their prospects in transistor electronics. Nanoscale 7, 8261–8283. https://doi.org/10.1039/C5NR01052G.

Sha, R., Vishnu, N., Badhulika, S., 2019. MoS_2 based ultra-low-cost, flexible, non-enzymatic and non-invasive electrochemical sensor for highly selective detection of uric acid in human urine samples. Sens. Actuators B Chem. 279, 53–60. https://doi.org/10.1016/j.snb.2018.09.106.

Shan, J., Li, J., Chu, X., Xu, M., Jin, F., Wang, X., 2018. High sensitivity glucose detection at extremely low concentrations using a MoS_2-based field-effect transistor. RSC Adv. 7942–7948.

Somani, P.R., Somani, S.P., Umeno, M., 2006. Planer nano-graphenes from camphor by CVD. Chem. Phys. Lett. 430, 56–59. https://doi.org/10.1016/j.cplett.2006.06.081.

Soni, A., Pandey, C.M., Pandey, M.K., Sumana, G., 2018. Highly efficient polyaniline-MoS_2 hybrid nanostructures based biosensor for cancer biomarker detection. Anal. Chim. Acta ⟨https://doi.org/S000326701831482X⟩.

Su, S., Sun, H., Xu, F., Yuwen, L., Wang, L., 2013. Highly sensitive and selective determination of dopamine in the presence of ascorbic acid using gold nanoparticles-decorated MoS_2 nanosheets modified electrode. Electroanalysis 1–7. https://doi.org/10.1002/elan.201300332.

Su, S., Sun, H., Cao, W., Chao, J., Peng, H., Zuo, X., Yuwen, L., Fan, C., Wang, L., 2016. Dual-target electrochemical biosensing based on DNA structural switching on gold nanoparticle-decorated MoS_2 nanosheets. ACS Appl. Mater. Interfaces 8, 6826–6833. https://doi.org/10.1021/acsami.5b12833.

Sun, J., Lindvall, N., Cole, M.T., Wang, T., Booth, T.J., Bggild, P., Teo, K.B.K., Liu, J., Yurgens, A., 2012. Controllable chemical vapor deposition of large area uniform nanocrystalline graphene directly on silicon dioxide. J. Appl. Phys. 111. https://doi.org/10.1063/1.3686135.

Swaminathan, H., Balasubramanian, K., 2018. Forster resonance energy transfer between MoS_2 quantum dots and polyaniline for turn-on bovine serum albumin sensing. Sens. Actuators B. Chem. 264, 337–343. https://doi.org/10.1016/j.snb.2018.02.182.

Syahir, A., Usui, K., Tomizaki, K., Kajikawa, K., Mihara, H., 2015. Label and kabel-free detection techniques for protein microarrays. Microarrays 4, 228–244. https://doi.org/10.3390/microarrays4020228.

Tan, C., Cao, X., Wu, X.J., He, Q., Yang, J., Zhang, X., Chen, J., Zhao, W., Han, S., Nam, G.H., Sindoro, M., Zhang, H., 2017. Recent advances in ultrathin two-dimensional nanomaterials. Chem. Rev. 117, 6225–6331. https://doi.org/10.1021/acs.chemrev.6b00558.

Taniselass, S., Arshad, M.K.M., Gopinath, S.C.B., 2019. Graphene-based electrochemical biosensors for monitoring noncommunicable disease biomarkers. Biosens. Bioelectron. 130, 276–292. https://doi.org/10.1016/j.bios.2019.01.047.

Wachter, S., Polyushkin, D.K., Bethge, O., Mueller, T., 2017. A microprocessor based on a two-dimensional semiconductor. Nat. Commun. 8, 1–6. https://doi.org/10.1038/ncomms14948.

Wang, J., Tan, X., Pang, X., Liu, L., Tan, F., Li, N., 2016. MoS_2 quantum dot@polyaniline onorganic-organic nanohybrids for in vivo dual-modal imaging guided synergistic photothermal/radiation therapy. ACS Appl. Mater. Interfaces 8, 24331–24338. https://doi.org/10.1021/acsami.6b08391.

Wang, L., Wang, Y., Wong, J.I., Palacios, T., Kong, J., Yang, H.Y., 2014. Functionalized MoS_2 nanosheet-based field-effect biosensor for label-free sensitive detection of cancer marker proteins in solution. Small 10, 1101–1105. https://doi.org/10.1002/smll.201302081.

Wang, T., Zhu, H., Zhuo, J., Zhu, Z., Papakonstantinou, P., Lubarsky, G., Lin, J., Li, M., 2013. Biosensor based on ultrasmall MoS_2 nanoparticles for electrochemical detection of H2O2 released by cells at the nanomolar level. Anal. Chem. 85, 10289–10295. https://doi.org/10.1021/ac402114c.

Wang, Y., Ni, Y., 2014. Molybdenum disulfide quantum dots as a photoluminescence sensing platform for 2, 4, 6-trinitrophenol detection. Anal. Chem. 86, 7463–7470.

Wang, Y., Du, Y., Deng, J., Wang, Z., 2019. Friction reduction of water based lubricant with highly dispersed functional MoS_2 nanosheets. Colloids Surf. A 562, 321–328. https://doi.org/10.1016/j.colsurfa.2018.11.047.

Wang, Y.H., Huang, K.J., Wu, X., 2017. Recent advances in transition-metal dichalcogenides based electrochemical biosensors: a review. Biosens. Bioelectron. 97, 305–316. https://doi.org/10.1016/j.bios.2017.06.011.

Wang, Z., Mi, B., 2017. Environmental applications of 2D molybdenum disulfide (MoS_2) nanosheets. Environ. Sci. Technol. 51, 8229–8244. https://doi.org/10.1021/acs.est.7b01466.

Wiśniewska-Weinert, H., 2013. Exfoliation based technology of large scale manufacturing molybdenum disulphide graphene-like nanoparticle mixtures. Arch. Civ. Mech. Eng. 13, 144–149. https://doi.org/10.1016/j.acme.2013.01.007.

Xiang, X., Shi, J., Huang, F., Zheng, M., Deng, Q., Xu, J., 2015. MoS_2 nanosheet-based fluorescent biosensor for protein detection via terminal protection of small-molecule-linked DNA and exonuclease III-aided DNA recycling amplification. Biosens. Bioelectron. 74, 227–232. https://doi.org/10.1016/j.bios.2015.06.045.

Yang, T., Chen, H., Ge, T., Wang, J., Li, W., Jiao, K., 2015. Highly sensitive determination of chloramphenicol based on thin-layered MoS_2/polyaniline nanocomposite. Talanta 144, 1324–1328. https://doi.org/10.1016/j.talanta.2015.08.004.

Yang, Y., Liu, T., Cheng, L., Song, G., Liu, Z., Chen, M., 2015. MoS_2-based nanoprobes for detection of silver ions in aqueous solutions and bacteria. ACS Appl. Mater. Interfaces 7, 7526–7533. https://doi.org/10.1021/acsami.5b01222.

Zabinski, J.S., Donley, M.S., Dyhouse, V.J., McDevitt, N.T., 1992. Chemical and tribological characterization of PbO-MoS_2 films grown by pulsed laser deposition. Thin Solid Films 214, 156–163. https://doi.org/10.1016/0040-6090(92)90764-3.

Zeng, L., Li, X., Fan, S., Zhang, M., Yin, Z., Tadé, M., 2019. Photo-driven bioelectrochemical photocathode with polydopamine-coated TiO_2 nanotubes for self-sustaining MoS_2 synthesis to facilitate hydrogen evolution. J. Power Sources 413, 310–317. https://doi.org/10.1016/j.jpowsour.2018.12.054.

Zeng, Z., Yin, Z., Huang, X., Li, H., He, Q., Lu, G., Boey, F., Zhang, H., 2011. Single-layer semiconducting nanosheets: high-yield preparation and device fabrication. Angew. Chem. - Int. Ed. 50, 11093–11097. https://doi.org/10.1002/anie.201106004.

Zhang, D., Sun, Y., Li, P., Zhang, Y., 2016. Facile fabrication of MoS_2-Modified SnO_2 hybrid nanocomposite for ultrasensitive humidity sensing. ACS Appl. Mater. Interfaces 8, 14142–14149. https://doi.org/10.1021/acsami.6b02206.

Zhang, H., Zhang, H., Aldalbahi, A., Zuo, X., Fan, C., Mi, X., 2016. Fluorescent biosensors enabled by graphene and graphene oxide. Biosens. Bioelectron. 89, 96–106. https://doi.org/10.1016/j.bios.2016.07.030.

Zhang, X., Wang, H., Zhang, X., Zhao, Z., Zhu, Y., 2019. A multifunctional super-hydrophobic coating based on PDA modified MoS_2 with anti-corrosion and wear resistance. Colloids Surf. A Physicochem. Eng. Asp. https://doi.org/10.1016/j.colsurfa.2019.02.016.

Zhang, Yulong, Liu, Zi, Zou, Lina, B.Y, 2012. A new voltammetry sensor platform for eriocitrin based on CoS2-MoS_2-PDDA-GR nanocomposite. Talanta 66, 737–743. https://doi.org/10.1016/j.talanta.2018.07.004.

Zheng, Z., Feng, Q., Li, J., Wang, C., 2015. The p-type MoS_2 nanocube modified poly (diallyl dimethyl ammonium chloride)-mesoporous carbon composites as a catalytic amplification platform for electrochemical detection of L-cysteine. Sens. Actuators, B Chem. 221, 1162–1169. https://doi.org/10.1016/j.snb.2015.07.069.

Zhou, Y., Liu, Y., Zhao, W., Xie, F., Xu, R., Li, B., Zhou, X., Shen, H., 2016. Growth of vertically aligned MoS_2 nanosheets on a Ti substrate through a self-supported bonding interface for high-performance lithium-ion batteries a general approach. J. Mater. Chem. A 4, 5932–5941. https://doi.org/10.1039/c6ta01116k.

Zhu, X., Liang, X., Fan, X., Su, X., 2017. Fabrication of flower-like MoS_2/TiO_2 hybrid as an anode material for lithium ion batteries. RSC Adv. 7, 38119–38124. https://doi.org/10.1039/C7RA06294J.